DESIGN OF PERMANENT MAGNET SYNCHRONOUS MOTOR FOR LOW SPEED APPLICATIONS WITH FRACTIONAL SLOT CONCENTRATED WINDINGS

Major Project Report

Submitted in Partial Fulfillment of the Requirements for the Degree of

Master of Technology

In

Electrical Engineering

(Power Electronics, Machines & Drives)

By

Vishal Dineshbhai Devdhar

(09MEE004)

Department of Electrical Engineering

Institute of Technology

NIRMA UNIVERSITY

AHMEDABAD 382 481

MAY 2011

CERTIFICATE

This is to certify that the Major Project Report entitled **"Design of Permanent Magnet Synchronous Motor for Low Speed Applications with Fractional Slot Concentrated Windings"** submitted by **Mr.Vishal Dineshbhai Devdhar (09MEE004)** towards the partial fulfillment of the requirements for the award of degree in **Master of Technology (Electrical Engineering)** in the field of **Power Electronics, Machines & Drives** of **Nirma University** is the record of work carried out by him under our supervision and guidance. The work submitted has in our opinion reached a level required for being accepted for examination. The results embodied in this major project work to the best of our knowledge have not been submitted to any other University or Institution for award of any degree or diploma.

Date:

External Guide

Prof. R. H. Patel

Ex. Assistant Professor

Institute of Technology

Nirma University

Ahmedabad

Head of Department

Department of Electrical Engineering

Institute of Technology

Nirma University

Ahmedabad

Director

Institute of Technology

Nirma University

Ahmedabad

Acknowledgements

Success of any work depends upon the dedication, sincerity and hard work. It also requires some ingredients such as motivation, guidance, encouragement and time.

I wish to express my deepest gratitude to my project guide Prof. R. H. Patel, Ex. Assistant professor, Department of Electrical Engineering, Institute of Technology, Nirma University, Ahmedabad, for her constant guidance, encouragement and support. I warmly acknowledge and express my special thanks for her inspiring discussions and infallible suggestions.

I am also grateful to Dr.P. N. Tekwani, PG co-ordinator (PEMD), Department of Electrical Engineering, Institute of Technology, Nirma University, Ahmedabad, Prof.U. A. Patel, Section Head, Department of Electrical Engineering, Institute of Technology, Nirma University, Ahmedabad, Prof.A. S. Ranade, Head of Department, Department of Electrical Engineering, Institute of Technology, Nirma University, Ahmedabad, Dr.K. Kotecha, Director, Institute of Technology, Nirma University, Ahmedabad for giving me opportunity to perform the project under the premises of Institute of Technology, Nirma University, Ahmedabad.

Also I would like to thank to the other faculty members Dr.S C Vora, Dr.J G Jamnani, Prof.A N Patel, Prof.M T Shah, Prof.T H Panchal, Prof.V B Pandya, Prof.P N Kapil and Prof.S N Jani of Department of Electrical Engineering, Institute of Technology, Nirma University, Ahmedabad for their evaluation, helping understanding the subject and suggestions.

I wish to express my special thanks to lab assistants Pratik A Jani, Mohmadsajid M Chauhan, Hitesh M Makwana and Harshad K Patel for their day to day help during the project work.

I also wish to express my gratitude to my parents (Dineshbhai & Nayanaben), sister (Meghna) and grandfather (Babulal M Devdhar) for their support and sacrifices for me. I would also like to thank my friends Mihir, Krunal, Dhruv, Avdhut, Ruchit, Niti and Purvi for their help and understanding during the work.

Also I would like to thank all who have directly or indirectly helped me during the project work. Last but not the least I would like to thank the Almighty for providing me mental and physical strength to carry out the project work in time.

- Vishal D Devdhar

Ahmedabad

May - 2011

Abstract

This thesis covers the design of permanent magnet synchronous motor (PMSM) with fractional slot concentrated windings (FSCW). PMSMs with FSCW are most suitable for low speed direct drive applications. PMSMs with FSCWs offer advantages like; high pole number with less number of slots and shorter end turn length of the windings, which ultimately decreases the amount of copper to be used.

The specifications of PMSM are 45 kW, 400 rpm, and 1000 Nm, specifically used for pulp and paper industry applications.

Analytic design of PMSMs with different slot/pole combinations is carried out with motor design software. The main concern was to find a machine design that resulted in a low amount of airgap flux density harmonics. In order to find a suitable design, the machine performance was studied for different slot/pole combinations. Thus a low airgap flux density harmonic in the machine with 48/40 slot/pole combination is obtained. Special attention is given to the airgap flux density harmonics of the machine. This selected design is studied with finite element method (FEM) in order to verify the analytical results. A comparison is made between analytical design and FEM simulation, the result shows acceptable correlation, leading to the fulfillments of the requirements.

Further optimization of the design to reduce airgap flux density harmonics is carried out with the FEM simulations. The design is optimized thorough shaping of permanent magnet and varying the stator slot opening width methods.

List of Figures

3.1 a)Conventional geared drive with Induction Motor, b) Direct drive with PM machine . . . 13
3.2 Wind turbine directly coupled to a generator . . . 14
3.3 Marine propulsion system . . . 15
3.4 Conventional washing machine drive . . . 16
3.5 Direct drive washing machine . . . 16

4.1 Radial-flux inner rotor PM synchronous machines . . . 20
4.2 Surface mounted PMSM . . . 21
4.3 Inset PMSM . . . 22
4.4 Buried PMSM . . . 22
4.5 End windings of one phase of 10-pole machines: a) a traditional onelayer winding with $Q_s = 30$ and $q = 1$, b) a one-layer fractional winding $Q_s = 12$ and $q = 0.4$ and c) a two-layer fractional slot winding with $Q_s = 12$ and $q = 0.4$, where the slot is divided vertically [7]. . . . 23
4.6 Surface PM machine with two types of concentrated stator windings: single-layer (left) and double-layer (right) [8]. . . . 24

5.1 PMSM geometrical parameters. . . . 26
5.2 Cross-section of one pole of a four pole SMPM with relevant geometrical parameters. . . . 27
5.3 Illustration of the dimensions in the area of the stator slot opening. . 29
5.4 Actual and fundamental airgap flux density. . . . 29
5.5 Phasor diagram of non-salient PMSM at rated speed. . . . 31
5.6 Drive for PMSM. . . . 32
5.7 Stator inner diameter v/s Motor torque . . . 37
5.8 Winding schematic: a) concentrated, b) distributed . . . 38

6.1 Flux density produced by a main pole . . . 41
6.2 Airgap magnet flux density of 24/16 motor . . . 43
6.3 Airgap magnet flux density of 24/20 motor . . . 43
6.4 Airgap magnet flux density of 24/28 motor . . . 43
6.5 Airgap magnet flux density of 36/24 motor . . . 44
6.6 Airgap magnet flux density of 48/32 motor . . . 44

6.7 Airgap magnet flux density of 48/40 motor 44
6.8 Airgap flux density of 24/16 motor 45
6.9 Airgap flux density of 24/20 motor 45
6.10 Airgap flux density of 24/28 motor 46
6.11 Airgap flux density of 36/24 motor 46
6.12 Airgap flux density of 48/32 motor 47
6.13 Airgap flux density of 48/40 motor 47
6.14 Airgap flux density harmonic plot of 24/16 motor 48
6.15 Airgap flux density harmonic plot of 24/20 motor 48
6.16 Airgap flux density harmonic plot of 24/28 motor 49
6.17 Airgap flux density harmonic plot of 36/24 motor 49
6.18 Airgap flux density harmonic plot of 48/32 motor 50
6.19 Airgap flux density harmonic plot of 48/40 motor 50
6.20 Comparison of airgap flux density %THD 51

7.1 Cross section view of 48/40 PMSM 56
7.2 2D FE model of 48/40 PMSM 57
7.3 3D FE model of 48/40 PMSM 58
7.4 Meshing of PMSM model 58
7.5 Flux contour plot (Magnified View) 59
7.6 Flux density plot 60
7.7 Flux density plot (Magnified View) 61
7.8 Flux density arrow plot 61
7.9 Instantaneous magnetic energy 62
7.10 Instantaneous magnetic co-energy 62
7.11 Torque about origin (Transient Analysis) 63
7.12 Torque v/s Rotor position 63

8.1 Airgap flux density 65
8.2 FFT of Airgap flux density 65
8.3 Slot opening width with 5mm 66
8.4 Slot opening width with 1mm 66
8.5 Airgap flux density with slot opening 1mm 67
8.6 Magnet shape and magnetization 67
8.7 Airgap flux for different magnetization 68
8.8 Simple magnet shape as main pole 69
8.9 Bread loaf type magnet shape as main pole 69
8.10 Airgap flux density with bread loaf magnet 69
8.11 Comparison of FFT of airgap flux density 70

List of Tables

5.1 Machine constant parameters 37
5.2 Slot/pole combinations for PMSM 39
5.3 Winding factors of different motors 40

6.1 % THD of the airgap flux density 51

7.1 Geometry parameters 56
7.2 Flux density comparison 60

Nomenclature

Greek Symbols

α	half pole angle in electrical degrees	[°]
β	angle between the d-axis and the current vector	$[rad]$
δ	airgap length	$[m]$
δ_e	equivalent airgap	$[m]$
γ	current angle between the line current I and the induced voltage E	$[rad]$
μ_0	magnetic permeability of free space ($4\pi \times 10^{-7}$)	[H/m]
μ_r	relative magnet permeability	-
Φ	flux	$[Wb]$
Ψ_m	magnet flux linkage	$[Wb]$
τ	average pole pitch	$[m]$
τ_s	stator slot pitch	$[m]$
θ	angular coordinate	$[rad]$
ω	electrical angular frequency	[Hz]

Symbols

A_{sl}	slot area	$[m^2]$
$\hat{B}_\delta$	amplitude of the fundamental airgap flux density	$[T]$
B_m	maximum value of the airgap flux density	$[T]$
B_r	remanence flux density of the permanent magnet	$[T]$
B_{ry}	flux density in the rotor yoke	$[T]$
B_{sy}	flux density in stator core	$[T]$
B_{ts}	flux density in a stator tooth	$[T]$
b_{so}	stator slot opening	$[m]$
b_{ss1}	inner stator slot width	$[m]$
b_{ss2}	outer stator slot width	$[m]$
b_{ts}	stator tooth width	$[m]$
D	inner stator diameter	$[m]$
D_{rc}	outer rotor diameter	$[m]$
D_i	inner rotor diameter	$[m]$
D_o	outer stator diameter	$[m]$
E	fundamental of the induced voltage (RMS value)	$[V]$
f	frequency	$[Hz]$
SF_g	slot fill factor	-
h_{ry}	rotor yoke height	$[m]$
h_{ss}	stator slot height	$[m]$
h_{sw}	slot wedge height	$[m]$
h_m	magnet thickness	$[m]$

I	line current	$[A]$
I_d	d-axis current	$[A]$
I_q	q-axis current	$[A]$
J	current density	$[A/m^2]$
k	integer	-
k_c	Carter factor	-
k_{coil}	end-winding coefficient	-
k_{core}	correction factor for the calculation of the current loading	-
k_{leak}	correction factor for the airgap flux density calculation	-
$k_{leaktooth}$	correction factor for the flux density in the teeth	-
k_{open}	ratio of the slot opening over the slot width	-
k_{w1}	fundamental winding factor	-
L	active length	$[m]$
L_d	d-axis inductance	$[H]$
L_{md}	d-axis magnetizing inductance	$[H]$
L_{mq}	q-axis magnetizing inductance	$[H]$
L_q	q-axis inductance	$[H]$
m	number of phases	-
m_a	amplitude modulation ratio	-
n	synchronous speed	$[rpm]$
n_s	number of conductors per slot	-
p	number of poles	-
q	number of slots per pole per phase	-
Q_s	number of stator slots	-
R	resistance of one phase of the stator winding	$[\Omega]$
S_1	current loading	$[A/m]$
T	torque	$[Nm]$
V	external voltage	$[V]$
V_d	rectified voltage across the filter capacitor	$[V]$
X_{md}	armature reaction reactance	$[\Omega]$
X_d	d-axis synchronous reactance	$[\Omega]$
X_l	leakage reactance	$[\Omega]$

Abbreviations

AFPM ..... Axial-Flux Permanent Magnet
BLDC ..... Brush Less DC
EMF ..... Electro Motive Force
FEA ..... Finite Element Analysis
FFT ..... Fast Fourier Transform
FSCW ..... Fractional Slot Concentrated Winding
NdFeB ..... Neodymium Iron Boron
PDE ..... Partial Differential Equation
PM ..... Permanent Magnet
PMSM ..... Permanent Magnet Synchronous Motor
RFPM ..... Radial Flux Permanent Magnet
RMS ..... Root Mean Square
SMPM ..... Surface Mounted Permanent Magnet
TFPM ..... Transverse-Flux Permanent Magnet
THD ..... Total Harmonic Distortion

Contents

Acknowledgements **i**

Abstract **iii**

List of Figures **iv**

List of Tables **vi**

Nomenclature **vii**

Abbreviations **ix**

Contents **x**

1 Introduction **1**
1.1 Background 1
1.2 Problem identification 2
1.2.1 Number of poles 2
1.3 Possible solution 3
1.4 Main contribution of the thesis 3
1.5 Outline of the thesis 3

2 Literature Survey **5**

3 Low Speed Direct Drives **12**
3.1 Advantages of direct drives 12
3.2 Examples of low speed direct drive applications 14
3.2.1 Wind turbine 14
3.2.2 Marine propulsion 15
3.2.3 Washing machines 15
3.2.4 Pulp and paper industry 17
3.2.5 Waste-water treatment plant mixer 17
3.2.6 Others 17
3.3 Motor topology 18

3.4 Active weight and iron losses 18

4 Permanent Magnet Synchronous Motor & Fractional Slot Concentrated Winding 19
4.1 Radial-flux inner rotor PM synchronous machines 19
4.2 Types of PMSM 19
4.2.1 Surface-mounted PMSM 20
4.2.2 Inset PMSM 21
4.2.3 Buried PMSM 21
4.3 Fractional slot concentrated winding 23

5 Analytical Design 25
5.1 Geometrical properties 25
5.2 Magnetic properties 28
5.2.1 Analytic calculation of airgap flux density 28
5.2.2 Analytic calculation of teeth flux density 30
5.3 Electrical properties 31
5.3.1 Inductances 31
5.3.2 Resistance of one phase of the stator winding 32
5.3.3 The external voltage 32
5.3.4 Induced voltage 33
5.3.5 Ampere-turns per slot 33
5.3.6 Number of conductors per slot 34
5.4 Proposed PMSM design 36
5.4.1 Winding 38

6 Harmonic Analysis and Results 41
6.1 Airgap flux density harmonics 41
6.2 Simulation results 43
6.3 Choice of design 52

7 Finite Element Analysis 53
7.1 Basics of FEA 53
7.2 FEA simulation 55
7.2.1 Creating FE model 56
7.2.2 FEA simulation results 59

8 Harmonics in PMSM 64
8.1 Harmonic calculation 64
8.2 Harmonic reduction technique 66
8.2.1 Varying stator slot opening width 66
8.2.2 Shaping of permanent magnet 67
8.3 Result Comparison 70

9 Conclusion and Future Scope **71**
9.1 Conclusion 71
9.2 Future scope 72

References **73**

List of Publication **77**

Chapter 1

Introduction

1.1 Background

Induction motors are the most widely used motors in the industrial applications because of their simple construction, low maintenance, no commutator, low price and moderate reliability. The disadvantages are the possibility of cracking the rotor bars due to hot spots at plugging and reversal, and lower efficiency and power factor than synchronous motors. As environmental concern increases, electrical drives with higher efficiency are desirable. The use of permanent magnet materials in electrical machines have been known for a long time. But due to the low energy product of the ferrite materials used at that time the use was limited to low power machines. However, frequency converters and new materials bring new possibilities for the machine designers.

New permanent magnet materials with high energy product have been commercially developed. This started a large-scale development of the permanent magnet synchronous machines. Thus, replacing conventional induction machines with permanent magnet synchronous machine (PMSM) has recently gained great interest. The PMSM is essentially a synchronous machine where the excitation winding is replaced with permanent magnets. PM machines have no rotor winding which results in lower

copper losses and therefore feature a higher efficiency than induction machines. High efficiency and accurate control of the machines are more important in industrial applications.

For low-speed applications, below 500 rpm, PM machines may further eliminate the need of a gearbox. To adapt the speed and torque of the machine, a gearbox is traditionally coupled to a standard induction machine. It is advantageous to remove this mechanical element because it is costly, decreases the drive efficiency, and needs maintenance. Low-speed (or high-speed) drives without a gearbox are termed direct drives, since the machines are directly coupled to the load.

1.2 Problem identification

1.2.1 Number of poles

The fundamental frequency f of the power-electronic converter is given by the required speed of the synchronous motor (n in rpm) and its number of poles p:

$$n = \frac{120\, f}{p} \tag{1.1}$$

Machines with a low number of poles, designed for a higher rated speed, can be operated at low speeds if the supplied frequency is low, as long as the mechanical structure and shaft of the machine can cope with the higher torque. However, this solution is not efficient since the supplied frequency gets much lower than the rated frequency range of the converter. With a low frequency, the transistors have to be over-dimensioned in order to withstand the larger thermal variations. Therefore, machines with a high number of poles are generally preferable. The advantage of

high pole number is a low iron mass per rated torque due to rather low flux per pole. A high pole number in conventional wound machines leads also to a high slot number, which increases costs and in the worst cases leads to a low copper fill factor (the amount of insulation material compared to the slot area is big) [2].

1.3 Possible solution

To reduce the number of slots although the number of poles is higher the fractional slot winding solution is the best option. Less number of slots reduces both the iron and the copper mass in the machine which reduces overall cost. The fractional slot winding allows a longer stator stack in the same frame length than conventional windings since the axial length of end winding is typically smaller [2].

1.4 Main contribution of the thesis

This thesis mainly deals with the design of permanent magnet synchronous motor. The PMSM used for the pulp and paper industry applications is the interest of this thesis. Low speed large torque drive is the requirement of the application selected. The fractional slot concentrated winding is to be used. The FSCW produce harmonics and these harmonics should be eliminated. The objective of the thesis is to reduce the airgap flux density harmonics by varying the motor slot/pole combination and further elimination of the harmonics with slot and magnet shape optimization using finite element analysis (FEA).

1.5 Outline of the thesis

Chapter 2 gives the thorough literature survey of PMSM with fractional slot windings and concentrated windings.

Chapter 3 discusses the low speed direct drives with its advantages and various industrial applications.

Chapter 4 describes the basics of the PMSM and fractional slot concentrated windings.

Chapter 5 gives the analytic design of PMSM and the proposed PMSM design with different slot/pole combinations.

Chapter 6 shows the airgap flux density harmonic equations and results of the simulations of the motor design software.

Chapter 7 describes the FEA simulations and verification of the analytical design with FEA results.

Chapter 8 shows the optimization results of the airgap flux density harmonics with FEA.

Chapter 9 refers to the conclusion and the future scope of the thesis.

Chapter 2

Literature Survey

High-power density and efficiency resulting from elimination of rotor windings and reduced magnetic flux losses have made PMSM popular. For low speed, high torque, direct drive, applications PMSM is best suited. As the speed of the motor is less, high pole number has to be chosen. High pole number increases the number of slots which increases the overall cost of the motor. For high pole machine, in order to reduce the slot number, fractional slot winding is the best option. The fractional slot concentrated windings have been gaining a lot of interest because of various advantages they provide. In this chapter literature survey of the fractional slot concentrated winding (FSCW) PMSM has been carried out. Several key publications on the surface mounted PMSM for low speed applications and FSCW are presented.

1 **Jerome Cros and Philippe Viarouge, "Synthesis of High Performance PM Motors with Concentrated Windings", IEEE Transactions on Energy Conversion, Vol. 17, NO. 2, pp. 248-253, June 2002.**

   Paper [1] deals with the synthesis of the three-phase structures with concentrated windings which demonstrates the performances of these machines compared to traditional machines with one slot per pole and per phase. The performances of the machines with concentrated windings are higher than the performances of the traditional machines, because the minimization of both copper

volume and Joule losses are reducing the manufacturing costs and improving the output characteristics.

2 **Pia Salminen, Markku Niemel, Juha Pyrhnen and Juhani Mantere, "Performance analysis of fractional slot wound PM-motors for low speed applications", IAS 2004, 0-7803-8486-5/04/$20.00 ©2004 IEEE, pp. 1032-1037.**

In [2] for 10 pole PMSM different windings layout and the copper amount of a fractional slot machine were studied and the results were compared to integer slotted machine. It was noticed that in fractional slot machines the flux density waveform is far away from the sinusoidal waveform, but regardless of that in some constructions the induced back EMF verified by FEM computations and measurements - is very sinusoidal and that means that it is possible to achieve a smooth torque.

3 **Pragasen Pillay, "Application Characteristics of Permanent Magnet Synchronous and Brushless dc Motors for Servo Drives", IEEE Transactions on Industry Applications, Vol. 21, No. 5, pp. 986-996, September/October 1991.**

In [3] the application characteristics of the PMSM & BDCM are discussed with the specified engineering selection criteria in this paper. For flux weakening operation PMSM is preferred. The surface mounted PM motor is less sensitive to parameter changes than buried PM machines.

4 **Li Xiao-hai , Zhu Li, Zhao Ji-min, Jiang Shu-zhong, "Research on Special Low-Speed, High-Torque Permanent Magnet Synchronous Motor for Screw Pump", IPEMC2009, 978-1-4244-3557-9/09/$25.00 ©2009 IEEE, pp. 1858-1862.**

Paper[4] investigates a special low-speed, high-torque PMSM to directly drive the screw pump without gear box. The cogging torque is the main obstacle for

the low speed, high torque PMSM. To reduce the cogging torque combination of fractional slot and optimized pole-arc coefficient is adopted. The analytical expression of cogging torque is also given based on the motor's model for analysis.

5 Xu Yanliang Sun Yuanyuan, "Fractional-slot Low Speed Large Torque Permanent Magnet Brushless Motors", ICIEA 2009, 978-1-4244-2800-7/09/$25.00 ©2009 IEEE, pp.3565-3569.

In [5] the performance of the fractional slot low speed large torque permanent magnet brushless motor (PMBM), which have the different slot number per pole per phase (q) of equal to or less than unit, but the same main dimensions, electromagnetic parameters and rated ones, are valuated comparatively. From the results it is obtained that the PMBM with fractional slot concentrated winding can characterized high flux weakening potential and high fault tolerance, enjoys a well sinusoidal no-load back EMF despite the possible trapezoid no-load air-gap flux density distribution.

6 Pia Marjatta Lindh, Hanne Kaarina Jussila, Markku Niemela, Asko Parviainen, and Juha Pyrhnen, "Comparison of Concentrated Winding Permanent Magnet Motors With Embedded and Surface-Mounted Rotor Magnets", IEEE Transactions on Magnetics, Vol. 45, No. 5, pp. 2085-2089, May 2009.

Low-speed permanent magnet machines with concentrated windings aiming at a high efficiency and high torque per volume ratios are in the focus of paper [6]. Concentrated winding permanent magnet machines with embedded magnets or rotor surface magnets give good performance, when the number of slots per pole per phase is chosen to be either 0.4 or 0.5. Rotor surface magnet motors with semi-closed slots give smaller losses than rotor surface magnet motors with open slots.

7 H. Jussila, P. Salminen, M. Niemela and J.Pyrhonen, "Guidelines for Designing Concentrated Winding Fractional Slot Permanent Magnet Machines", POWERENG 2007, April 12-14, 2007, Setbal, Portugal, 1-4244-0895-4/07/$20.00 ©2007 IEEE, pp. 191-194.

Paper [7] discusses the guidelines for designing concentrated winding fractional slot permanent magnet machines. In this paper the winding factor, unwanted magnetic pull, pull out torque, cogging torque and torque ripple are analyzed. A machine with q = 0.4 has a relatively good winding factor and pull-put torque (p.u) and a low cogging torque and torque ripple.

8 Jian Gao, Yanan Yu, Shoudao Huang, "Winding Layers and Slot/Pole Combination in Fractional Slot/Pole PMSM - Effects on Motor Performance", IEEE Explore.

Paper [8] mainly studies the performance of fractional Slot/Pole PMSM due to different winding layer and slot/pole combinations. Through finite element analysis, it is shown that the using of close slot/pole combination could reduce cogging torque effectively, meanwhile double-layer winding could reduce torque ripple effectively when using of close slot/pole combination.

9 Ayman M. El-Refaie, and Thomas M. Jahns, "Impact of Winding Layer Number and Magnet Type on Synchronous Surface PM Machines Designed for Wide Constant-Power Range Operation" IEEE Transaction on Energy Conversion, Vol. 23, No. 1, pp. 53-60, March 2008.

Paper [9] thoroughly investigates the impact of the winding layer number and the choice of magnet type on the performance characteristics of surface permanent magnet (SPM) machines with fractional slot concentrated windings designed for wide speed ranges of constant-power operation. Here three different machines are compared according to magnet type and winding layer. Machines

with double-layer stator windings have lower spatial subharmonic components in their stator airgap MMF distributions, resulting in lower torque ripple and magnet eddy current losses compared to the single-layer winding designs.

10 **J. A. Gemes, A. M. Iraolagoitia, M. P. Donsin, and J. I. Del Hoyo, "Analysis of Torque in Permanent Magnet Synchronous Motors with Fractional Slot Windings", Proceedings of the 2008 International Conference on Electrical Machines, Paper ID 1181, 978-1-4244-1736-0/08/$25.00 ©2008 IEEE, pp.1-4.**

In [10] by utilizing the finite element technique the influence of various types of windings on the cogging torque and torque developed by a PMSM has been investigated. The 24-slot motor has lower cogging torque and higher average electromagnetic torque than the 48-slot motor. The torque ripple of the 48-slot motors is much lower than for the 24-slot machine. Optimizing the cogging torque to a low value is therefore not sufficient to obtain a low torque ripple.

11 **G. Sooriyakumar, R. Perryman and S. J. Dodds, "Cogging Torque Analysis for Fractional Slot/Pole Permanent Magnet Synchronous Motors", UPEC 2007, pp. 188-191.**

Analytical and FEA predictions of cogging torque are compared with experimental results for a range of non-skewed PMSMs of similar size but with slot/pole ratios of 18/8, 12/10 and 30/8 (fractional) together with 30/10 and 18/6 (integer) in the paper [11]. Even though the cogging torque is less in the 30-8 design compared to all the other designs, the 12-10 design is preferred for production since it has a significantly higher torque density while producing a cogging torque at an acceptable level.

12 **J. H. Walker and N. Kerruish, "Design of Fractional Slot Windings", The Institution of Electrical Engineers, Paper No. 2678 S, pp. 428-440, Aug. 1958.**

A simple method of calculating the electrical design of a fractional- slot winding and of determining the amplitude of the subharmonics and harmonics generated in the air-gap flux-density are presented in [12].

13 Mircea Popescu, David G. Dorrell, Dan Ionel and Calum Cossar, "Single and Double Layer Windings in Fractional Slot-per-Pole PM Machines - Effects on Motor Performance", 978-1-4244-1-1766-7/08/ $25.00 ©2008 IEEE, pp. 2055-2060.

Paper [13] discusses the effects of fractional slots per pole in brushless permanent magnet motors. Machines with different poles numbers and single or double layer concentrated winding are compared and the performance is investigated in terms of winding MMF harmonic and torque production. The 16 and 20 pole machines have a very low cogging torque and prototype motors have significant magnet leakage across the tooth tip because the pole and slot numbers are close.

14 Nicola Bianchi, Silverio Bolognani, and Michele Dai Pr, "Magnetic Loading of Fractional-Slot Three-Phase PM Motors With Nonoverlapped Coils", IEEE Transactions on Industry Applications, Vol. 44, No. 5, pp. 1513-1521, September/October 2008.

Paper [14] deals with the magnetic analysis and design of fractional-slot PM motors with nonoverlapped coils. Here the several issues have been considered such as double and single layer windings, the MMF harmonic contents, the zero mutual coupling among the phases, the peak magnetic potential due to the stator currents.

15 P. Salminen, M. Niemel, J. Pyrhnen and J. Mantere, "High-Torque Low-Torque-Ripple Fractional-Slot PM-Motors", 0-7803-8987-5/05/ $20.00 ©2005 IEEE, pp. 144-148.

In [15] several slot-pole-combinations are studied and compared with each other for the torque ripple values and the pull-out torques of the fractional slot PM

Motors. The analyses of these computations give new information on the character of fractional slot machines and some guiding criteria for choosing a suitable slot-pole combination to be used for the application concerned. Low torque ripples were reported with machines having several slots and poles, e.g. 36-slots and 30 or 42 poles. Although a high fundamental winding factor is used, this does not guarantee that the machine will have the capacity of producing a high torque.

16 Manoj R. Shah and Ayman M. EL-Refaie, "End Effects in Multi-Phase Fractional-Slot Concentrated-Winding Surface Permanent Magnet Synchronous Machines", 978-1-4244-2893-9/09/$25.00 2009 IEEE, pp. 3798-3805.

Paper [16] investigated the end effects in Fractional-slot concentrated-winding PMSM. The study focuses on eddy current losses in the frame, end shields, and clamping rings (magnetic/nonmagnetic.). Desirable slot/pole combinations for different number of phases are investigated including both the single and the double layer windings. SL windings produce significantly higher losses compared to DL windings. Going to higher number of phases could have a detrimental effect in terms of increasing the losses or increasing the support structure size and weight along with other dynamics challenges.

17 Nicola Bianchi, Silverio Bolognani, Michele Dai Pr, and Giorgio Grezzani, "Design considerations for fractional-slot winding configurations of synchronous machines," IEEE Trans. Ind. Appl., vol. 42, no. 4, pp. 997-1006, Jul./Aug. 2006.

Paper [17] presents some design considerations for synchronous machines characterized by a fractional number of slots per pole per phase. The main advantage of this configuration is a smooth torque, which is due to the elimination of periodicity between slots and poles. A second advantage is a higher fault-tolerant capability, making the machine able to work even in faulty conditions.

Chapter 3

Low Speed Direct Drives

In this chapter the low speed direct drives are discussed. The advantages of direct drive has been presented with the different applications. Finally, some features specific to low-speed electrical machines for direct-drive applications are presented.

3.1 Advantages of direct drives

Many applications requires low rotating speed and a high torque. Usually, conventional induction machines with speeds from 1000 to 3000 rpm are connected to gearboxes, in order to achieve the required low speed and high torque as shown in fig.3.1(a). The emergence of PM machine technology offers today another alternative. PM machines can rotate directly at low speed and high torque, making it possible to eliminate the gearbox in the drive as shown in fig.3.1(b).
The advantages of direct drives are as follows:

- **Reduced maintenance -** A gearbox requires maintenance. Indeed, it needs to be regularly lubricated in order to minimize friction.

- **Higher reliability -** Without gearbox, important sources of failures are eliminated and the drive can have a longer lifetime.

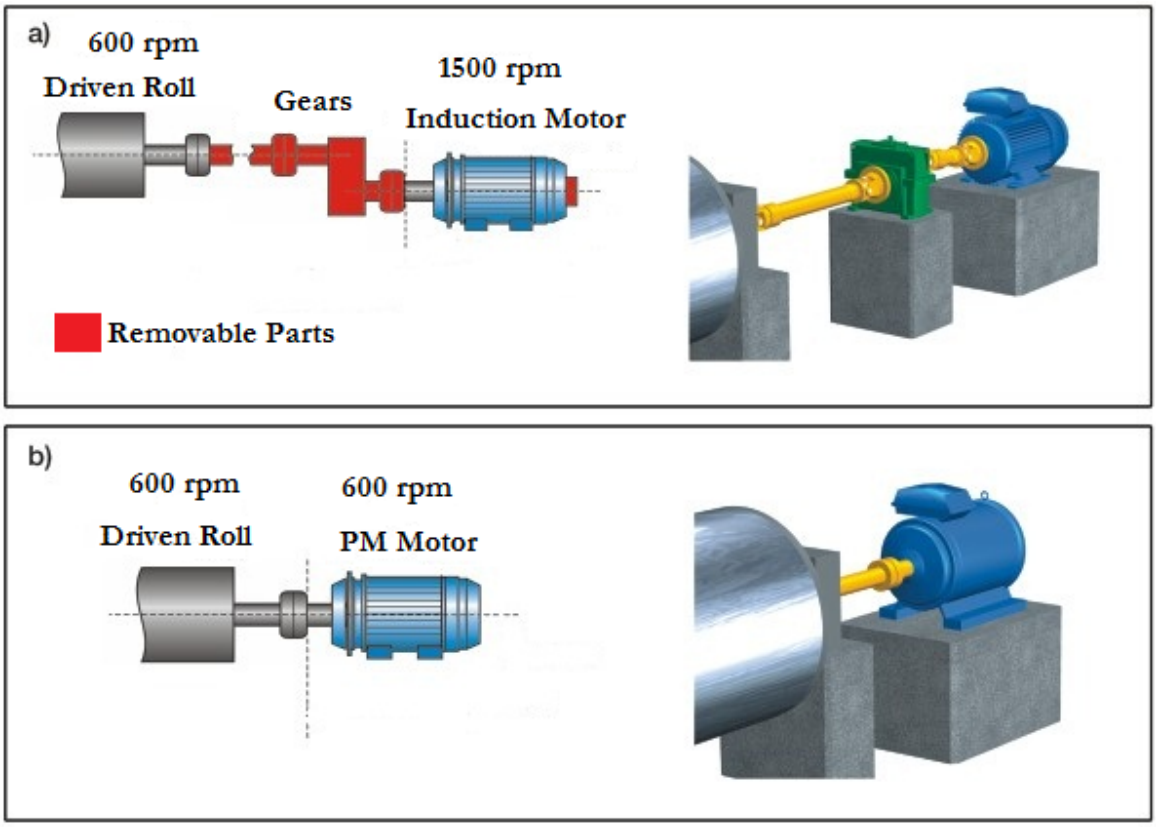

Figure 3.1: a)Conventional geared drive with Induction Motor, b) Direct drive with PM machine

- **Reduced noise -** A gearbox and other mechanical parts of the transmission system such as belts or pulleys are sources of noise. With fewer mechanical parts, the direct drives may thus be less noisy.

- **Higher efficiency -** Removing the gearbox means also removing a potential source of losses. The losses in the gearbox are mostly generated by friction between the gears.

- **Reduced weight -** A direct drive can be made lighter than a geared drive.

3.2 Examples of low speed direct drive applications

3.2.1 Wind turbine

Wind turbines are the source of nonconventional energy sources. Wind turbine installation is increasing day by day. Most of the installed wind turbines have a gearbox enabling a generator rotating at high speeds. In case of wind turbines, the main benefit of a direct drive is the reduction of failures and maintenance. The gearbox is responsible for the failure of the system most of the times. Depending on the turbine size, the power of the generator can be from a few kilowatts to several megawatts. So it is beneficial to couple a generator with a turbine directly to the shaft.

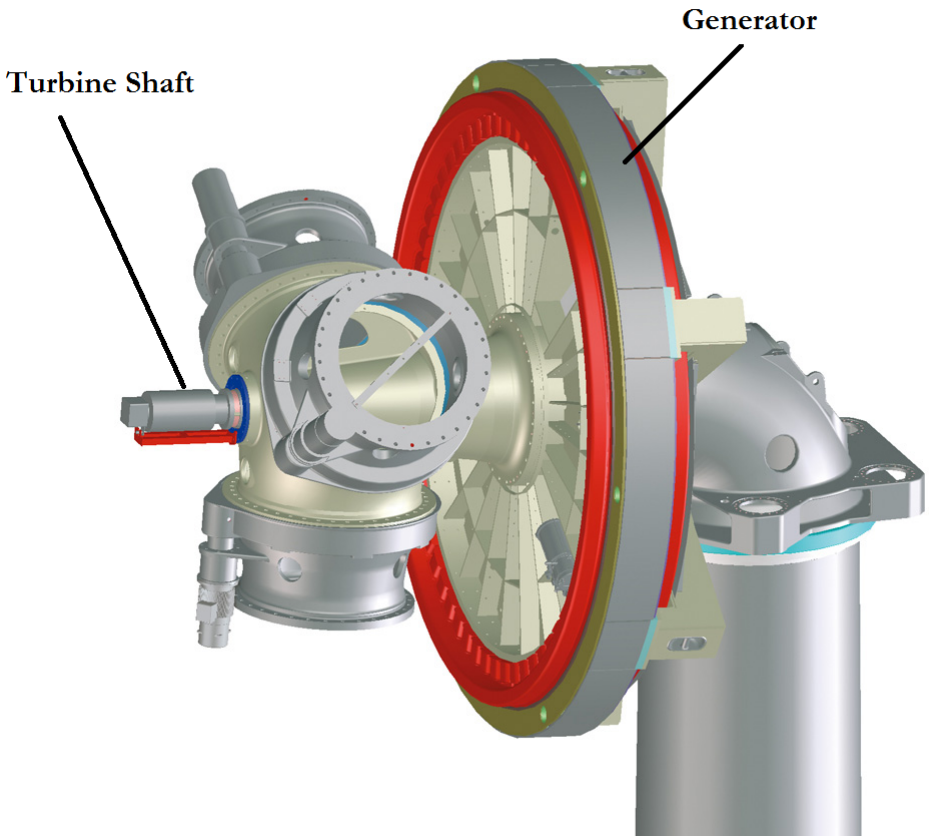

Figure 3.2: Wind turbine directly coupled to a generator

3.2.2 Marine propulsion

Most of the cruise ships manufactured today have an electric propulsion. Among other advantages, the electric propulsion offers a better passenger comfort and is more reliable than conventional drives with diesel engines or gas turbines[18]. Direct-drive PM motors also tend to replace synchronous machines connected to gearboxes. For this application, the main advantages of the direct drive is its lower weight and the gain in maneuverability for the ship. The PM motor can be placed in a rotatable pod directly connected to the propeller which makes it possible to change the position of the propeller (and thus of the ship) very easily and smoothly.

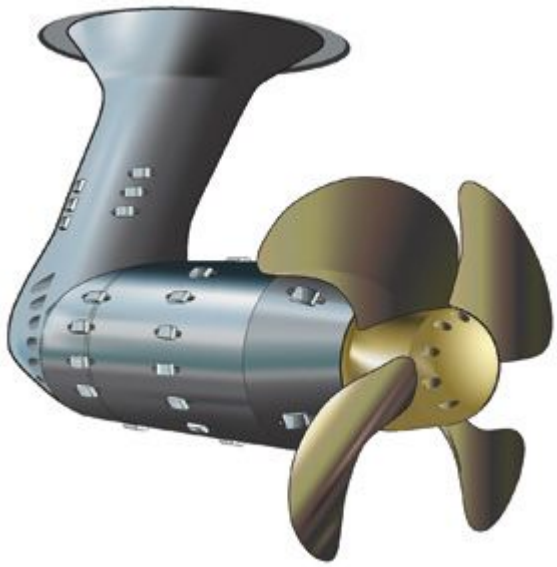

Figure 3.3: Marine propulsion system

3.2.3 Washing machines

In a conventional washing machine, a DC or an induction motor drives the drum via a belt and pulleys as shown in fig.3.4. The main advantage of a direct-drive washing machine as showm in fig.3.5 comes from the suppression of the belt, pulley and eventual brushes of the DC motor. Indeed, these elements are the weak parts of

the washing machine and are often the cause of failures. A washing-machine motor for home appliance rates usually less than one kilowatt. The drum of the machine rotates approximately at 50 rpm during the washing process, up to approximately 1500 rpm or higher during the drain [18]. Therefore, the direct-drive motor of the washing machine should run over a large speed range which is achieved by operating under field-weakening. LG produces the most famous commercialized direct-drive washing machine for home appliances. The motor, directly-connected to the drum, is a brushless DC (BLDC) PM motor as shown in fig. 3.5.

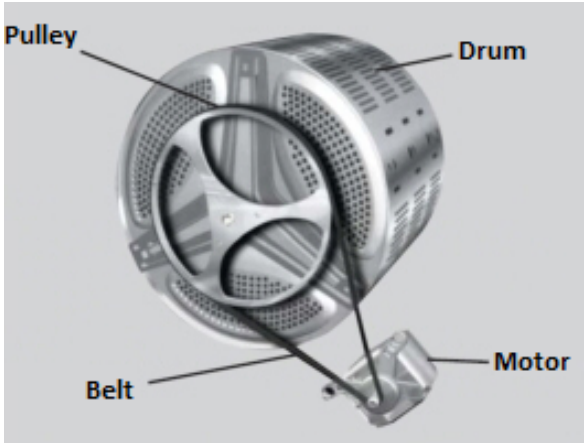

Figure 3.4: Conventional washing machine drive

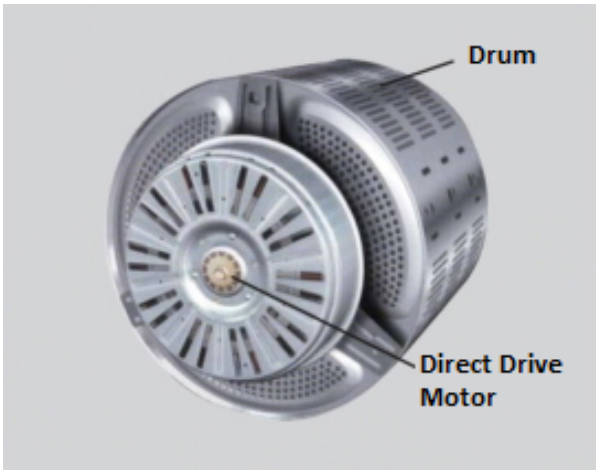

Figure 3.5: Direct drive washing machine

3.2.4 Pulp and paper industry

Low-speed drives with gearboxes are widely used in the pulp and paper industry. However, a direct drive without gearbox allows, among other advantages, a gain of space and an easier installation. Paper machines have rotational speeds between 200 and 600 rpm. Motor powers range from 30 kW to 1800 kW [18]. Direct drives with induction motors can compete with geared drives in some cases. PMSM are also successfully used in direct drives for pulp and paper applications. These machines are Radial flux PM (RFPM) motors.

3.2.5 Waste-water treatment plant mixer

During the process of cleaning waste-water, mixers are used in large pools in order to keep the fluid in movement. This mixers are driven by induction motor coupled to a gear box. The advantages with using a direct-drive mixer include an increased efficiency and the introduction of speed control which gives the user a higher flexibility. Low-speed waste-water mixers have rated powers of a few kilowatts. The direct-drive mixer costs more than the geared mixer. However, it has a better efficiency. The geared mixers drive has an efficiency of 73% against 80% for the direct drive [18]. A PMSM for a low-speed direct-drive 4.5kW waste-water treatment mixer has been investigated and designed in [18].

3.2.6 Others

Direct drives are also becoming more common in applications requiring precise speed and position controls. Such applications include machine tools, turning tables, radar, telescopes, etc. The motors used in these applications are the so-called torque motors which are brushless DC servomotors with (usually) surface-mounted PMs on the rotor. In order to provide large torques, the torque motors have a large airgap diameter and, therefore, they look like a ring [18].

3.3 Motor topology

With induction machines, the power factor drops with higher pole numbers due to an increased leakage inductance. Therefore, induction machines are not really suitable for low-speed direct-drives. On the contrary, the power factor of PM machines is not affected in the same manner by their number of poles. With their high torque density, PM machines are, therefore, usually considered for low-speed direct drives. RFPM, axial-flux permanent magnet (AFPM) and transverse-flux permanent magnet (TFPM) machines are all suitable for low-speed direct drives. The focus in this thesis is on RFPM machines and the main reason is that AFPM and TFPM are complex to manufacture and the weight of the nonactive magnetic material is large and difficult to estimate [18].

3.4 Active weight and iron losses

PM machines with a high number of poles can feature a low active weight. Indeed, for the same required nominal torque, motors with a high number of poles have a lighter magnetic circuit than motors with few poles. The flux density is identical but the flux from one pole to the other is inversely proportional to the number of poles. Since the flux is lower with a higher number of poles, the stator and rotor yokes can be made thinner without any higher risk of saturating the iron.

As the active weight decreases with an increasing pole number. Since the volume of iron also decreases, the increase of the iron losses is limited when the frequency increases with the pole numbers. The iron losses increase more significantly due to the dependency on the frequency, since the frequency increases with the increasing pole number.

Chapter 4

Permanent Magnet Synchronous Motor & Fractional Slot Concentrated Winding

4.1 Radial-flux inner rotor PM synchronous machines

In radial-flux machines, the flux through the airgap flows in the radial direction while the current flows in the axial direction. This gives a resulting force on the rotor acting in the tangential direction as shown in fig.4.1. Radial-flux synchronous machines with inner rotor are the most commonly used permanent magnet machines. Radial-flux PM machines can be designed in several ways with different stator windings and different rotor configurations.

4.2 Types of PMSM

According to the location of permanent magnet on the rotor the PMSM are classified as :

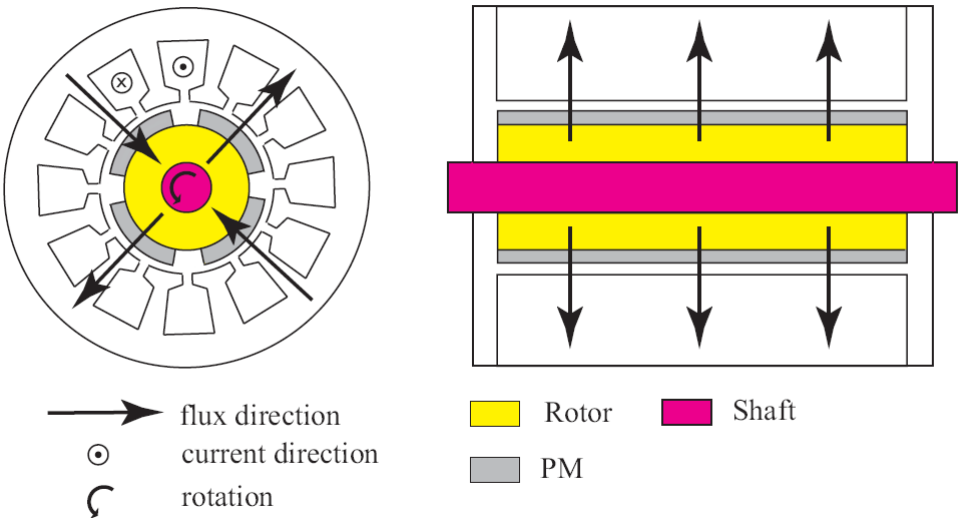

Figure 4.1: Radial-flux inner rotor PM synchronous machines

- Surface-mounted PMSM
- Inset PMSM
- Buried PMSM

4.2.1 Surface-mounted PMSM

Surface mounted permanent magnet (SMPM) is the most common rotor configuration for PM machines. The magnets are placed on the rotor surface as shown in fig.4.2. As the permeability of the magnets is almost the same as the permeability of air, the d-axis and the q-axis reluctances are equal. Hence, the SMPM machines have no saliency and the torque is produced by the interaction between the stator currents and the magnets only.

The main advantage of the SMPM machine is its simplicity and consequently its lower construction cost compared to other PM machines. The magnets are glued onto the rotor surface and fixed by a carbon or glass fiber bandage. In relation to other PM concepts, the surface mounted machines are easy to manufacture and consequently

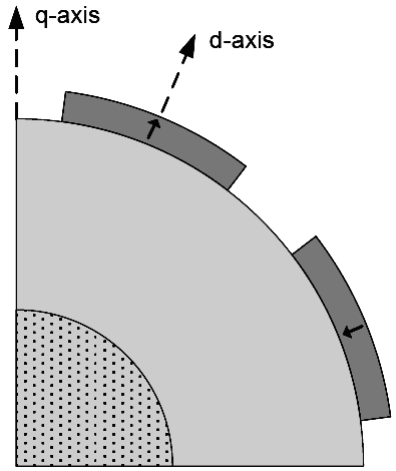

Figure 4.2: Surface mounted PMSM

the construction cost is lower. The main drawback of these machines is the exposition of the permanent magnets to demagnetization fields. Furthermore, the magnets are subject to centrifugal forces that can cause their detachment from the rotor.

4.2.2 Inset PMSM

In inset PM machines, the magnets are mounted on the rotor surface as shown in fig 4.3. But the magnets are sunken in the rotor core, offering better protection than in a SMPM machine. However, a bandage is often required in order to withstand the centrifugal forces. Due to the iron between the magnets, the q-axis reluctance is lower than the d-axis reluctance. This is known as salient poles. Due to the saliency, a reluctance torque is created in addition to the torque from the magnets.

4.2.3 Buried PMSM

Another PM concept is to bury the magnets in the rotor core as shown in fig. 4.4. This is referred to as buried PM machines. The magnets are better protected against demagnetization fields and mechanical stress. There are many different possibilities

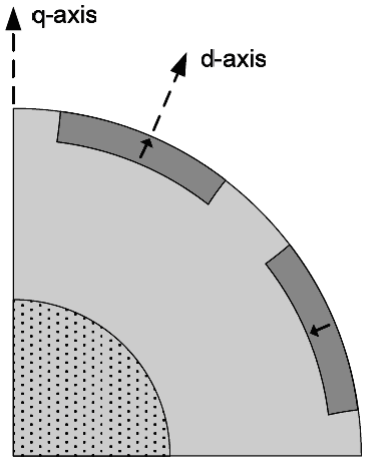

Figure 4.3: Inset PMSM

for the placement of magnets in the rotor. The magnets can be placed in such a way that the flux generated by the magnets in the rotor is concentrated and thus high airgap flux densities can be achieved. As the inset PM machines the buried PM machines have salient poles. A main drawback of the buried PM machines is the difficult manufacturing process and thus the high production cost.

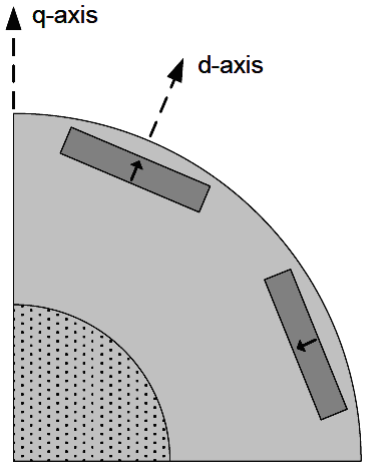

Figure 4.4: Buried PMSM

4.3 Fractional slot concentrated winding

The winding is called a fractional slot winding, if the number of slots per pole and per phase is not an integer number

$$q = \frac{Q_s}{p\,m} \tag{4.1}$$

Q_s is the number of stator slots, p is the rotor pole number and m is the number of stator phases. When each coil is wound around one tooth, the winding is called a concentrated winding. Such a permanent magnet machine may be used in low-speed applications, in which stator copper losses are dominating and iron losses are less important. In cases where the frequency of the stator is less than or equal to 100 Hz, the iron losses depending on the stator core material are typically not as significant as copper losses. The fractional slot PM synchronous machine produces some losses in the rotor and it is therefore inherently best suited for low speed applications [7].

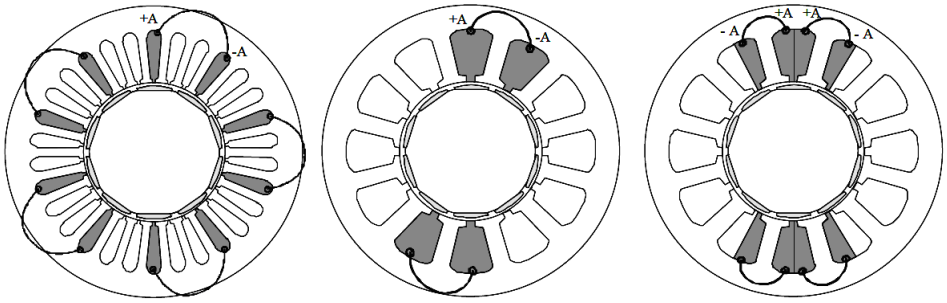

Figure 4.5: End windings of one phase of 10-pole machines: a) a traditional onelayer winding with $Q_s = 30$ and $q = 1$, b) a one-layer fractional winding $Q_s = 12$ and $q = 0.4$ and c) a two-layer fractional slot winding with $Q_s = 12$ and $q = 0.4$, where the slot is divided vertically [7].

It is easy to see that the end windings of the fractional slot concentrated windings are notably shorter than the end windings of integral slot windings. The insulation and manufacturing systems are also easier in the fractional slot windings since the end windings are not overlapping each other. The winding width may, however, be far less

than the pole pitch in these machines, which causes some inherent ineffectiveness in this machine type. The fractional slot windings may be divided into one-layer windings, fig. 4.5(b) or two-layer windings, fig. 4.5(c). In a two-layer winding, a slot is divided into two different parts, in which the coil sides may belong to different phases.

The following requirements or at least some of them are usually set for desirable machine constructions; the machine must have a large fundamental winding factor, it should produce the maximum torque and a low torque ripple, and further, unbalanced magnetic pull should be avoided and the machine should use a low amount of PM material. To achieve all these requirements, the best general choice could be a machine with $q = 0.4$. A machine with $q = 0.4$ has a relatively good winding factor and pull-put torque (p.u). The $q = 0.4$ machine could be a good choice because of the high torque ripple of the q = 0.5 machines [7]. Machines with $q = 0.33$ have the smallest cogging torque and torque ripple, but the pull-out torque (p.u) is also quite small. The $q = 0.4$ machine could be the best design to obtain a low cogging torque and torque ripple.

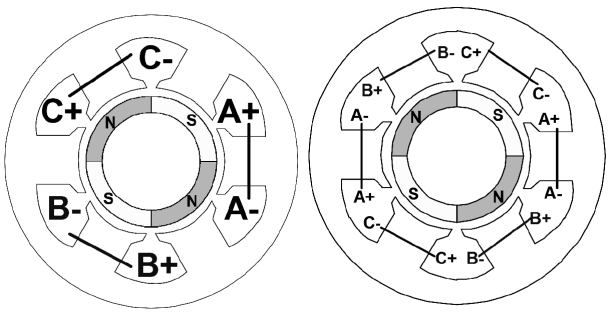

Figure 4.6: Surface PM machine with two types of concentrated stator windings: single-layer (left) and double-layer (right) [8].

The use of close slot/pole combination could reduce cogging torque effectively, meanwhile double-layer winding could reduce torque ripple effectively when using close slot/pole combination [8].

Chapter 5

Analytical Design

In this chapter the geometrical properties, magnetic properties and electric properties of PMSM are presented. The geometrical properties are the different dimensions and areas of the motor. The magnetic properties are the flux densities in the airgap and in the teeth. The electric properties are the inductances, resistances, ampere-turns and number of conductors per slot. Finally the proposed design of PMSM with specifications and constraints has been given.

5.1 Geometrical properties

The geometrical parameters of the motor configuration are presented in this section. Fig. 5.1 and 5.2 shows the geometry of a PMSM including the parameters of the geometrical dimensions.

$$D = D_{rc} + 2l_m + 2\delta \tag{5.1}$$

$$b_{ss1} = \pi \frac{D + 2h_{sw}}{Q_s} - b_{ts} \tag{5.2}$$

$$h_{sy} = \frac{1}{2}(D_o - D - 2h_{ss}) \tag{5.3}$$

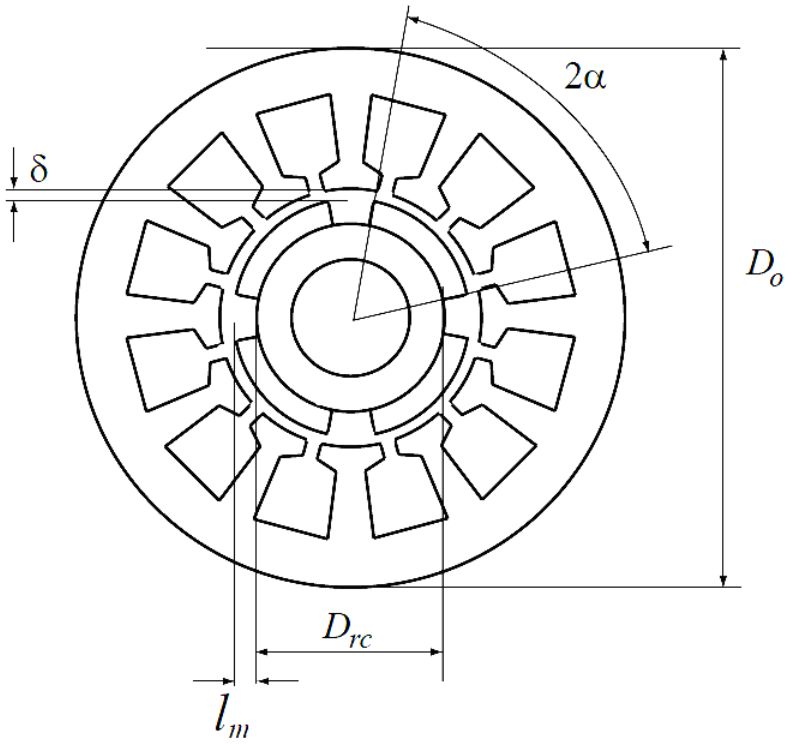

Figure 5.1: PMSM geometrical parameters.

$$b_{ss2} = \pi \frac{D + 2h_{ss}}{Q_s} - b_{ts} \tag{5.4}$$

$$k_{open} = \frac{b_{so}}{b_{ss1}} \tag{5.5}$$

This dimensions are expressed in equations 5.1 to 5.5, where Q_s is the number of stator slots. The parameter k_{open} is the ratio of the stator slot opening to the slot width 5.5. The teeth are straight, which means that the tooth width bts is constant all along the tooth. The inner stator diameter D is very large compared to the slot pitch τ_s. Therefore, b_{ss1}, b_{ss2} and b_{ts}, which actually are arcs of circle, are approximated as straight lines in equations 5.2 and 5.5. The slot area A_{sl} is given by equation 5.6.

$$A_{sl} = \frac{1}{2}(b_{ss1} + b_{ss2}) * (h_{ss} - h_{sw}) \tag{5.6}$$

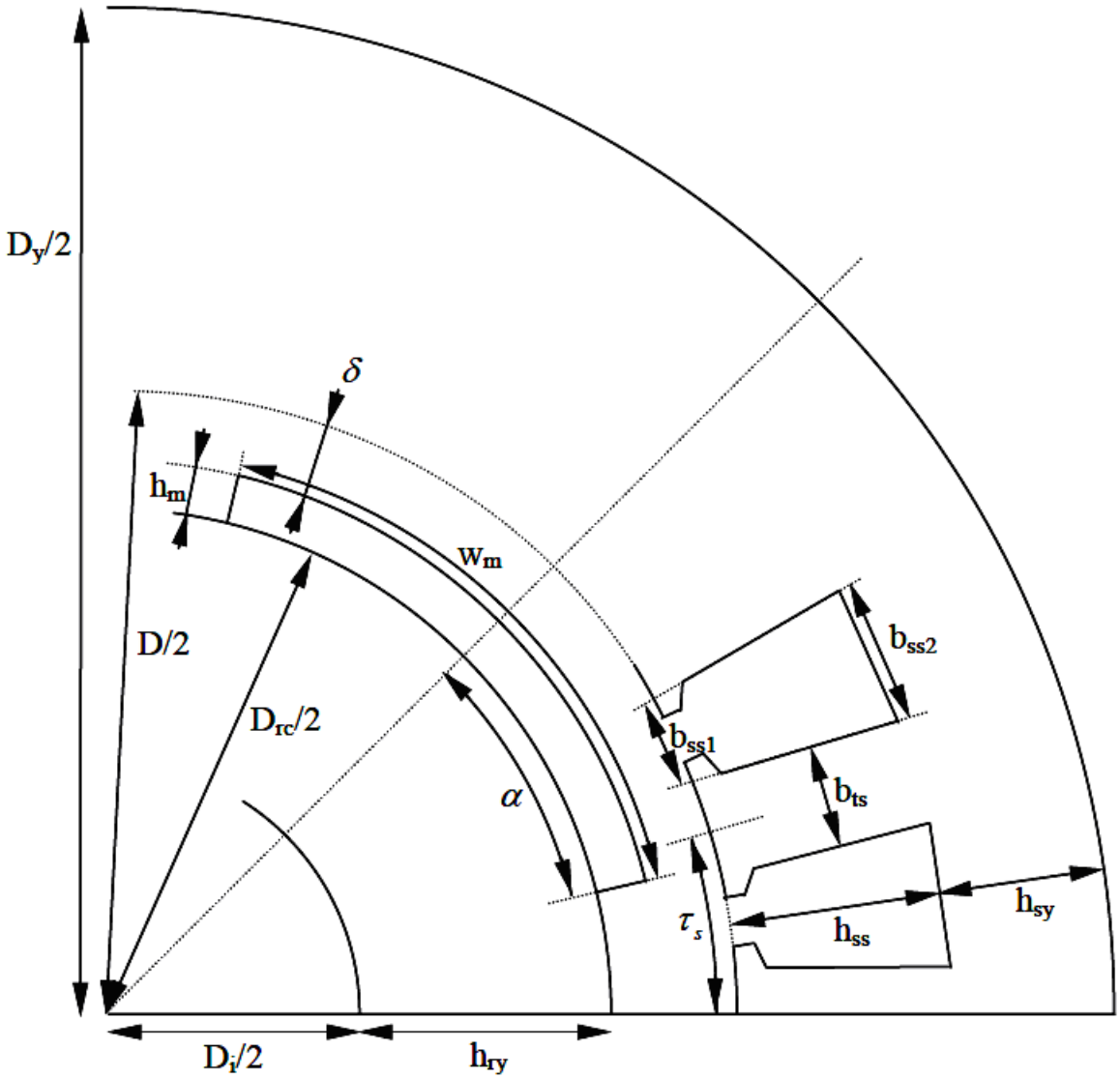

Figure 5.2: Cross-section of one pole of a four pole SMPM with relevant geometrical parameters.

According to the equations 5.1 to 5.6, the two-dimensional geometrical structure of the stator can be described entirely with the following parameters: D_{rc}, l_m, δ, h_{sw}, b_{ts}, D_o, h_{ss}, k_{open} and Q_s. Adding the number of poles p, the half pole angle α and the active length L, the whole three-dimensional geometry can be described (without considering the end-windings).

5.2 Magnetic properties

5.2.1 Analytic calculation of airgap flux density

The maximum value of the flux density in the airgap above the magnets (B_m) is given by the equation 5.7. It is assumed that the magnets are radially magnetized.

$$B_m = \frac{B_r \, k_{leak}}{1 + \frac{\mu_r \, \delta_e}{h_m}} \tag{5.7}$$

where δ_e is the equivalent airgap length and h_m is the magnet thickness. The factor k_{leak} is the ratio of the flux coupled with the stator windings to the total magnet flux. Consequently, k_{leak} is an empirical constant for taking the rotor flux leakage into account.

The equivalent airgap length is given by the equation 5.8

$$\delta_e = k_c \, \delta \tag{5.8}$$

which takes into account the effect of a slotted stator using the Carter factor k_c.

$$k_c = \frac{\tau_s}{\tau_s \; - \; \frac{(k_{open} b_{ss1})^2}{b_{ss1} k_{open} + 5\delta}} \tag{5.9}$$

The factor k_{leak} takes magnetic leakage between two neighboring permanent magnets into account.

$$k_{leak} = \frac{100 - (7p/60 \; - \; 0.5)}{100} \tag{5.10}$$

The definitions of the stator slot pitch τ_s, the inner stator slot width b_{ss1} and the stator opening factor k_{open} are shown in fig. 5.3 The stator slot pitch is calculated from the inner stator diameter D and the number of stator slots Q_s as follows:

$$\tau_s = \pi \frac{D - \delta}{Q_s} \tag{5.11}$$

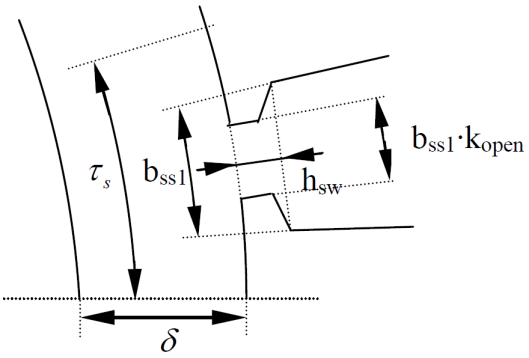

Figure 5.3: Illustration of the dimensions in the area of the stator slot opening.

The larger the airgap, the more magnet material is needed to produce the required airgap flux density. More magnet material implies not only a higher cost, but also a larger effective airgap. The positive effect of having a large airgap is that it gives a more sinusoidal flux distribution in the airgap, which results in a very small variation of flux density in the magnets and on the rotor surface. Thus, the eddy current losses (which are a function of the time rate of change of the vector flux density) can be significantly reduced.

Let us assume the airgap flux density has a rectangular shape as shown in fig. 5.4. The fundamental airgap flux density (B_δ) is then calculated to

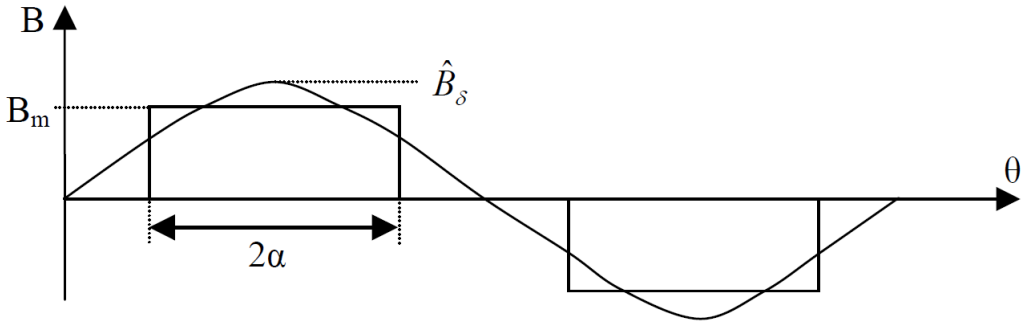

Figure 5.4: Actual and fundamental airgap flux density.

$$\hat{B}_\delta = \frac{4}{\pi} B_m \sin \alpha \tag{5.12}$$

where α is the half pole angle defined in electrical degrees:

$$\alpha = \frac{w_m\, p}{2(D - 2\delta)} \tag{5.13}$$

The pole angle (2δ) is two times the half pole angle and is normally chosen close to $2\pi/3$ electrical degrees (120^o). This can be explained by studying the fundamental component of the airgap flux density and its contribution to the torque of the motor. An increase of the pole angle to 180^o creates a 14 % higher airgap flux density as can be derived from equation 5.12, while the magnet volume increases by 50 %, which will approximately increase the cost of the magnets by the same percentage.

5.2.2 Analytic calculation of teeth flux density

The flux density in the tooth should be limited under the expected value otherwise the tooth can be saturated which means a higher magnetic leakage. The flux density in the teeth B_{ts} is calculated from the PM flux flowing through the airgap, the width of a tooth b_{ts} and the number of teeth through which the flux is flowing. Equation 5.14 gives the flux density in a tooth for a SMPM motor. The factor $k_{leaktooth}$ is used to take into account the part of leakage flux, flowing through the tooth shoe only.

$$B_{ts} = \frac{B_m 2\alpha \frac{2}{p}(\frac{D}{2} - \delta)(1 - k_{leaktooth})}{2b_{ts}} \tag{5.14}$$

$$k_{leaktooth} = \frac{17p/56 \; - \; 13/14}{100} \tag{5.15}$$

5.3 Electrical properties

The phasor diagrams for non-salient PM machines at rated speed are represented in fig. 5.5. SMPM motors are non-salient. The phasor diagram comprise of the d and$q$ axis inductances, L_d and L_q, the resistance of one phase of the stator winding R, the external voltage V, induced voltage E, angle between the flux from the permanent magnets Ψ_m and the current I.

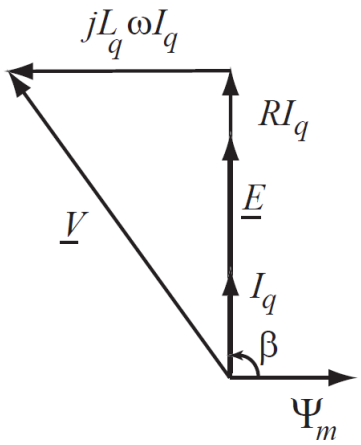

Figure 5.5: Phasor diagram of non-salient PMSM at rated speed.

5.3.1 Inductances

For a non salient motor the d and q axis synchronous inductances are equal

$$L_d = L_q = L_l + L_{md} = L_l + L_{mq} \tag{5.16}$$

where L_l is the leakage inductance and L_{md} and L_{mq} are the d- and q- axis magnetizing inductances respectively.

$$L_l = pqn_s^2 L\mu_0\lambda_1 \tag{5.17}$$

$$L_{md} = \frac{3}{\pi}(q n_s k_{w1})^2 \frac{\mu_0}{\delta k_c + \frac{l_m}{\mu_r}} (D - \delta) L \tag{5.18}$$

5.3.2 Resistance of one phase of the stator winding

It is assumed that all the coils in one phase are coupled in series. The phase resistance is calculated as:

$$R = \rho_{cu} \frac{(p\,L + (D + h_{ss})\pi\, k_{coil}) n_s^2\, q}{S F_g A_{sl}} \tag{5.19}$$

where SF_g is the slot fill factor. The end windings are taken into account by introducing the term k_{coil}.

5.3.3 The external voltage

Since all the investigated motor configurations are not self-starting, power electronic devices are essential to start the motor and make it rotate at the right speed.

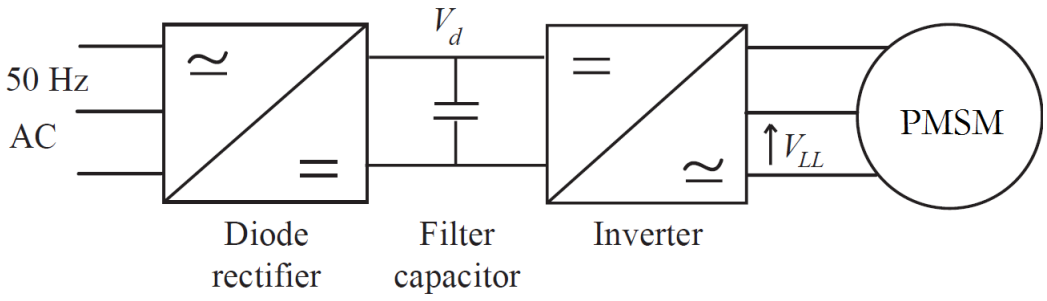

Figure 5.6: Drive for PMSM.

Fig. 5.6 shows a diagram of a simple drive that suits the application. A diode rectifier is coupled to a 3-phase inverter via a filter capacitor. The output line-to-line voltage V_{LL} of the inverter, which is also the voltage applied to the motor, can be estimated as:

$$V_{LL} = 0.612\, m_a\, V_d \tag{5.20}$$

where m_a is the amplitude modulation ratio of the inverter and V_d the rectified DC voltage across the filter capacitor. From the equation 5.20 a phase voltage V is calculated which is useful for number of conductors per slot of the motor.

5.3.4 Induced voltage

According to Faraday's law the induced voltage E is calculated from

$$E(t) = \frac{d\Psi_m}{dt} = N_s \frac{d\phi_m}{dt} \tag{5.21}$$

The maximum fundamental of the magnet flux $\hat{\phi_m}$ linked to one turn of the coil is:

$$\hat{\phi_m} = \frac{2}{\pi} \hat{B_\delta} L (D - \delta) \frac{\pi}{p} \tag{5.22}$$

N_s is the number of turns per phase which are in series:

$$N_s = \frac{p}{2} q \, n_s \tag{5.23}$$

Finally the rms-value of the induced voltage can be calculated as:

$$E = \frac{1}{\sqrt{2}} \, \omega \, k_{w1} \, q \, n_s \, \hat{B_\delta} \, L \, (D - \delta) \tag{5.24}$$

5.3.5 Ampere-turns per slot

Current loading

The peak value of the fundamental current loading S.1 is calculated from the torque equation:

$$\hat{S_1} = \frac{4\,T}{\pi \, (D - \delta)^2 \, L \, \hat{B_\delta} \, k_{w1} \, k_{cor} \, \sin \beta} \tag{5.25}$$

where β is the angle between Ψ_m and I. β depends on the saliency. For a non-salient geometry as the SMPM motor, β is $\frac{\pi}{2}$.
The correction factor k_{cor} is used to compensate the losses and leakages that are not analytically calculated, such as the flux leakage through the slots.

Current density From the fundamental peak current loading and the ampere-turns equation 5.26, the current density J can be calculated.

$$n_s\hat{I} = S_1\hat{\tau}_s \tag{5.26}$$

$$J = \frac{n_s I}{A_{sl} S F_g} \tag{5.27}$$

5.3.6 Number of conductors per slot

As equations 5.18 and 5.19 imply, the inductances and resistances depend on the square of the number of conductors per slot, whereas the induced voltage is linearly dependent on the number of conductors per slot (equation 5.21).

$$L_d = n_s^2 L_d^{'} \tag{5.28}$$

$$L_q = n_s^2 L_q^{'} \tag{5.29}$$

$$R = n_s^2 R^{'} \tag{5.30}$$

$$E = n_s E^{'} \tag{5.31}$$

From the phasor diagram of fig. 5.5 following equations are derived :

$$\hat{V^2} = (\hat{E} + RI_q)^2 \; + \; (L_d \, \omega \, I_q)^2 \tag{5.32}$$

From equations 5.28 to 5.31 the equation 5.32 becomes:

$$\hat{V^2} = (n_s \hat{E'} + n_s^2 R' \, I_q)^2 \; + \; (n_s^2 L_d^{'} \, \omega \, I_q)^2 \tag{5.33}$$

$$\hat{V^2} = n_s^2 (\hat{E'} + R^{'} (n_s I_q))^2 \; + \; n_s^2 (L_d^{'} \, \omega \, (n_s I_q))^2 \tag{5.34}$$

Finally, as $I_q = \hat{I}$, the number of conductor per slot :

$$n_s = \frac{\hat{V}}{\sqrt{(\hat{E'} + R' n_s \hat{I})^2 \; + \; (L_d^{'} \, \omega \, n_s \hat{I})^2}} \tag{5.35}$$

The equation 5.35 shows the total number of conductor per slot. To find the total number of conductors, total number of slots are required. From that total resistance can be calculated.

5.4 Proposed PMSM design

In this study PMSM specifications are selected for Pulp and Paper industry applications. In the Pulp and Paper industry the low speed motors are used. Conventionally the gear box is used to lower the speed below 500 rpm, replacing direct drive low speed PMSM can increase the efficiency of the drive.
The motor design specifications are :

- Rated power output = 45 kW
- Rated speed = 400 rpm
- Rated torque = 1000 Nm

To prevent the saturation and magnetic leakage, the flux density values are confined to some predetermined values. The reasonable design has the following magnetic characteristics:
Remanence flux density B_r = 1.2 T
Fundamental airgap flux density $\hat{B_\delta}$= 0.75 - 0.95 T
Maximum flux density in the rotor yoke B_{ry}= 1.4 T
Maximum flux density in the stator yoke B_{sy}= 1.7 T
Maximum flux density in the stator teeth B_{st}= 1.7 T
Relative magnet permeability μ_r= 1.05

To prevent the high temperatures and the insulation problems, the maximum current density J should be lower than 7 A/mm^2. This value is relevant for motor without forced cooling.

To select the diameter of the motor from the given specifications a computer program has been developed from the design equations. The values of different flux densities and the current loadings kept constant and the diameter of the motor was approx-

imated. Machine constant parameters are selected and the design of the motor is carried out with the motor designed software.

The selected machine constant parameters are given in the Table:5.1.

Table 5.1: Machine constant parameters

Stator stack length	L	140 mm
Stator stack outer diameter	D_o	400 mm
Stator stack inner diameter	D_i	282 mm
Slot fill factor	SF_g	0.4

The plot of Stator inner diameter v/s Motor torque obtain from computer program is shown in the 5.7. The torque values were varied and the specific electric and magnetic loadings were kept constant with the stack length.

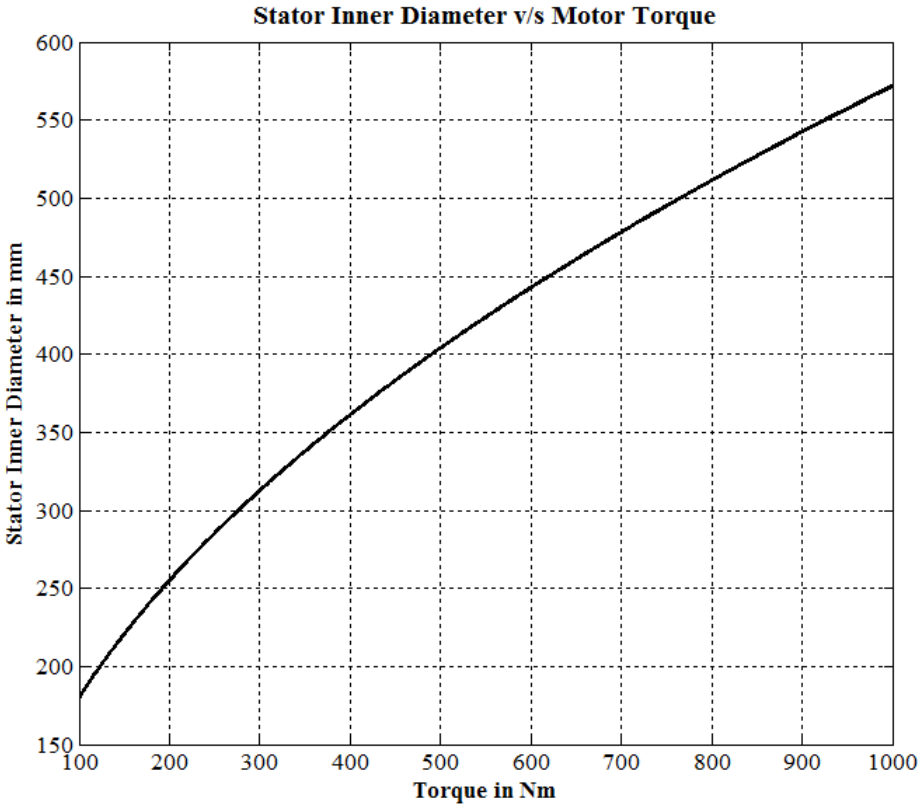

Figure 5.7: Stator inner diameter v/s Motor torque

5.4.1 Winding

The motor when used in low speed application, tends to choose a high pole number due to the good performances of low iron mass, low copper mass, low copper loss, low cost and high copper fill factor, if it at same time adopts winding configuration with q less than unit especially fractional-slot concentrated one. So winding configuration with $q < 1$ especially the fractional-slot concentrated one is focused greatly in low speed large torque direct-drive PMSM. It is possible to apply different windings in PMSMs, the concentrated winding and the distributed winding, which both have their own advantages and disadvantages.

The concentrated winding reduces the dimensions of the coil ends, and thus the copper losses, because end windings do not contribute to the torque generation but produce heat by copper losses. This forms a remarkable potential to reduce the portion of copper losses considerably. Less copper means also less total material cost, because copper is much more expensive than iron. Moreover, the concentrated winding significantly increases the space factor and extends the automated manufacturing because rectangular conductors, preformed coils and segmented cores are possible to apply. In concentrated winding the coil is wound around the tooth as shown in fig. 5.8.

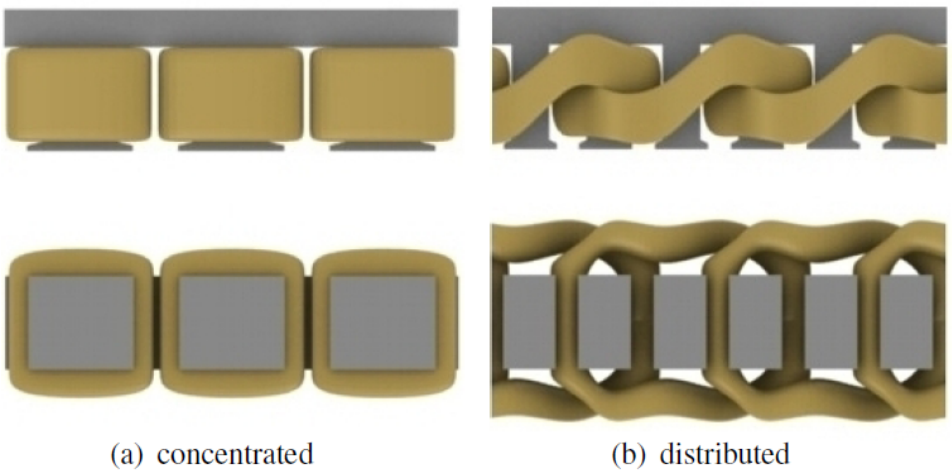

Figure 5.8: Winding schematic: a) concentrated, b) distributed

The design and analysis of FSCW PM machines is challenging in the sense that the winding configuration deviates significantly for the conventional sinusoidal distribution. This creates harmonics to the motor. These high harmonics increase the core loss, and decrease the efficiency of motor. On the other hand, it can bring about the fluctuation of the back EMF and winding phase current, then the electromagnetic torque ripple which directly causes vibration and noise is increased [21].

All the electromagnetic parameters of the PMSM, like core loss, electromagnetic torque and induced electromotive force EMF, are greatly dependent on the distribution of the air gap flux density, it directly affects the performance of the PMSM. In order to enhance efficiency and reduce vibration, the air gap flux density has to be optimized.

To reduce the harmonics and to optimize the airgap flux density, the different slot/pole combinations of the motor are analyzed and compared with each other, the slot/pole combination which produce lowest harmonic is selected. The different slot/pole combinations of the motors for the analysis are shown in 5.2.

Table 5.2: Slot/pole combinations for PMSM

Sr. No.	**No. of Slot**	**No. of Poles**	**Slot/Pole/Phase**	**Motor Name**
1	24	16	0.5	M1
2	24	20	0.4	M2
3	24	28	0.3	M3
4	36	24	0.5	M4
5	48	32	0.5	M5
6	48	40	0.4	M6

The motors with various slot/pole combinations are designed with the motor design software. Fractional slot concentrated winding is used for the design of all the motors given in Table:5.2. In the case of the Pulp and Paper Industry application, double-layer fractional slot concentrated windings are the most appropriate. Indeed, with the

lower harmonic content in the MMF, the losses and torque ripple are lower than with a single-layer winding. Furthermore, there are no requirement on a wide speed range of constant power operation and no constraints on fault tolerance. The motor constant parameters given in Table :5.1 and specifications are kept same for all the motors with different slot/pole combinations named M1 to M6 as mentioned in Table:5.2. The magnetic material used for the permanent magnet is NdFeB. The combinations of pole and slot numbers selected for the study, give high fundamental winding factors as discussed in [18]. The values of winding factors for different slot/pole combinations, selected for analysis are shown in Table:5.3.

Table 5.3: Winding factors of different motors

Sr. No.	**Motor**	**Winding Factor**
1	M1	0.866
2	M2	0.933
3	M3	0.933
4	M4	0.866
5	M5	0.866
6	M6	0.933

All the motors from M1 to M6 are designed and analyzed for the dynamic and harmonic analysis with the motor design software. The airgap flux density plots and harmonic analysis are shown in Chapter 6.

Chapter 6

Harmonic Analysis and Results

6.1 Airgap flux density harmonics

In the surface mounted PMSM the magnet pole thickness is h_m and its residual flux density is B_r, then the radial component of the air gap flux density can be expressed as given in [21].

$$B(\theta) = B_r \frac{h_m}{h_m + \delta(\theta)} \tag{6.1}$$

The air gap flux density wave form is assumed rectangular under the magnet pole. From fig.6.1, we can make a conclusion that the function of $B(\theta)$ is a periodic function whose period is $T = 2\tau_m$, so in the region of $(-T/2, T/2)$, its Fourier expansion can

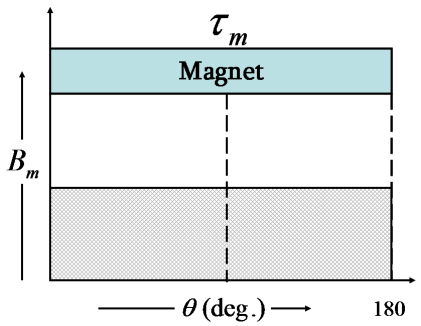

Figure 6.1: Flux density produced by a main pole

be written as

$$B_T(\theta) = \frac{a_0}{2} + \sum_{n=1}^{\infty}(a_n \cos nw\theta + b_n \sin nw\theta) \tag{6.2}$$

where n is the number of harmonics and $w = 2\pi/T$

$$a_0 = \frac{2}{T}\int_{-\frac{T}{2}}^{\frac{T}{2}} B(\theta)d\theta; \tag{6.3}$$

$$a_n = \frac{2}{T}\int_{-\frac{T}{2}}^{\frac{T}{2}} B(\theta)\cos nw\theta d\theta; \tag{6.4}$$

$$b_n = \frac{2}{T}\int_{-\frac{T}{2}}^{\frac{T}{2}} B(\theta)\sin nw\theta d\theta; \tag{6.5}$$

Where n=1,2,3...
as $a_0 = a_1 = a_2 = ...a_n = 0$;

$$b_n = \frac{4B_m}{n\pi}\cos n\alpha; \tag{6.6}$$

From the equations 6.2 and 6.6 the following expressions is obtained: the air gap flux density waveform under one pair of main pole produced by permanent magnet.

$$B_T = \frac{4B_m}{n\pi}\sum_{n=1,3,5...}^{\infty}\cos n\alpha \sin nw\theta; \tag{6.7}$$

The total harmonic distortion of air gap flux density is the percentage of square root of summation of all harmonic value squared to the square root of fundamental component and it is expressed by:

$$THD = \sqrt{\frac{\sum_{n=1,3,5...}^{\infty} B_n^2}{B_1^2}}; \tag{6.8}$$

6.2 Simulation results

Dynamic analysis of all the motors is carried out with the help of motor design software. From the dynamic analysis all the plots of flux densities are obtained. The magnet flux densities produced have the approximately rectangular shape as assumed. The flux density produced by the magnets are shown in the figures 6.2 to 6.7.

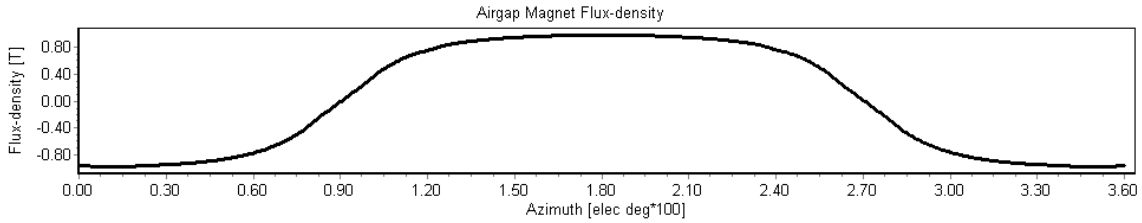

Figure 6.2: Airgap magnet flux density of 24/16 motor

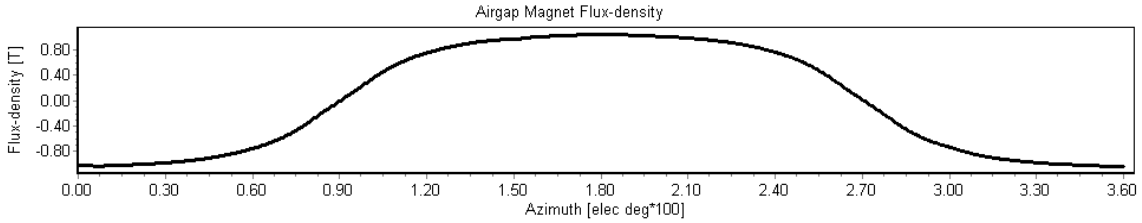

Figure 6.3: Airgap magnet flux density of 24/20 motor

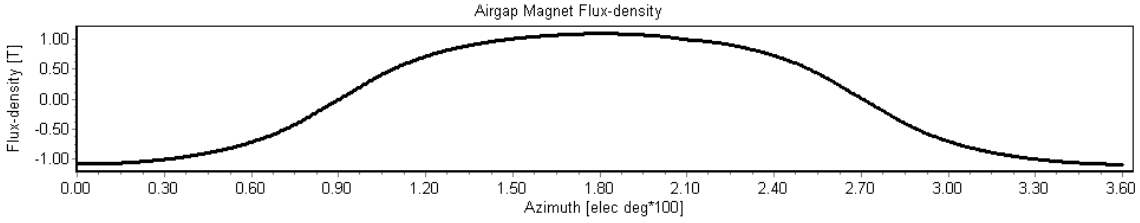

Figure 6.4: Airgap magnet flux density of 24/28 motor

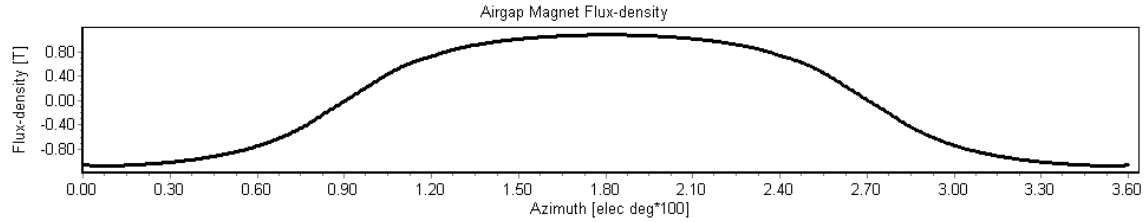

Figure 6.5: Airgap magnet flux density of 36/24 motor

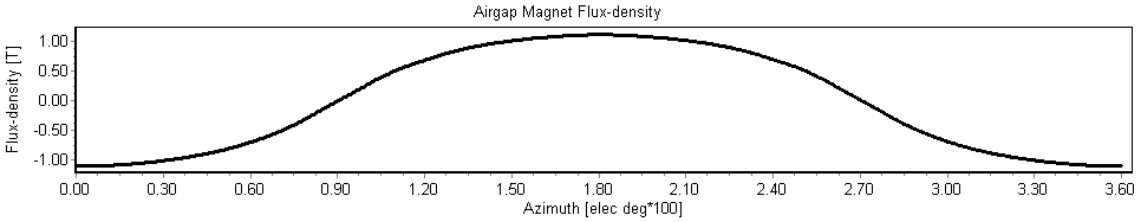

Figure 6.6: Airgap magnet flux density of 48/32 motor

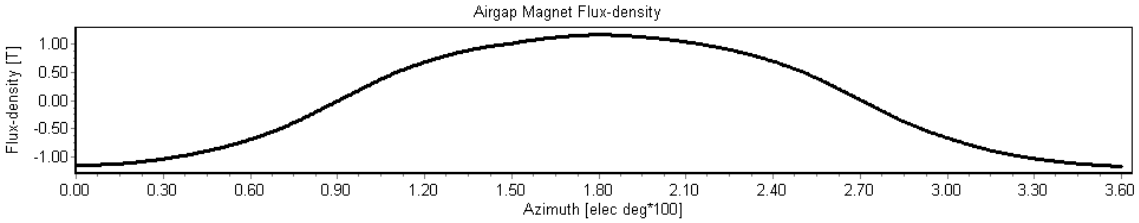

Figure 6.7: Airgap magnet flux density of 48/40 motor

The airgap flux density waveforms obtained by the dynamic analysis of the motors. From the observation of the airgap flux density waveforms of the different motors, it is seen that the shape of waveforms are not exactly sine wave but it is near to a sine wave. It shows the presence of the harmonics in the airgap flux density. The harmonic content is changing with the change of slot/pole combinations.

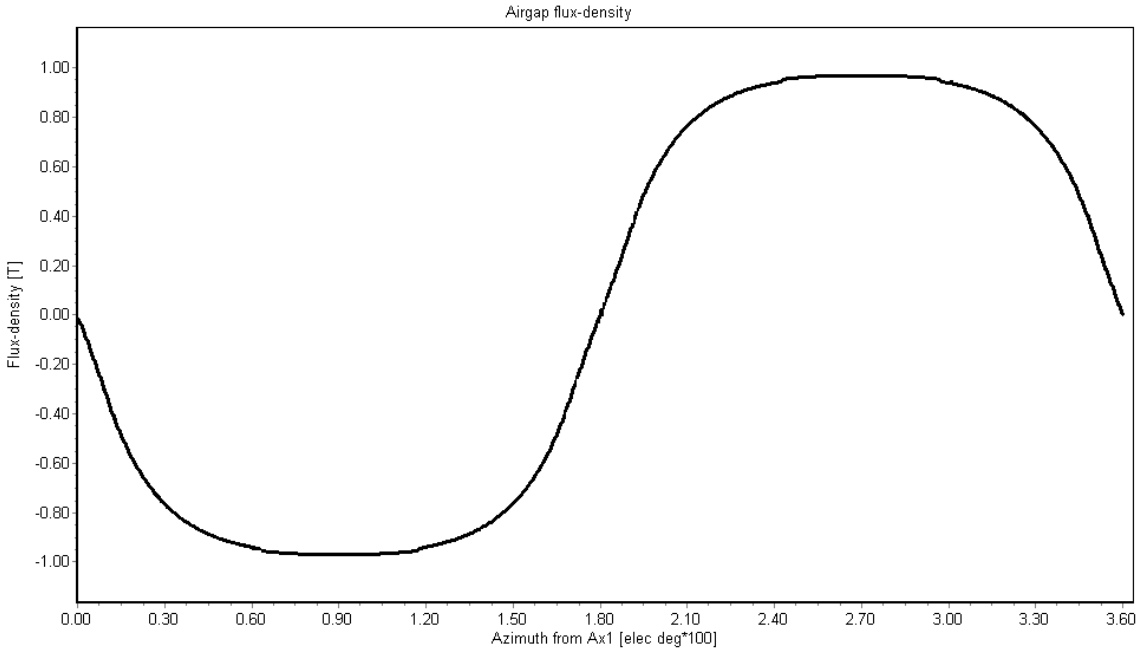

Figure 6.8: Airgap flux density of 24/16 motor

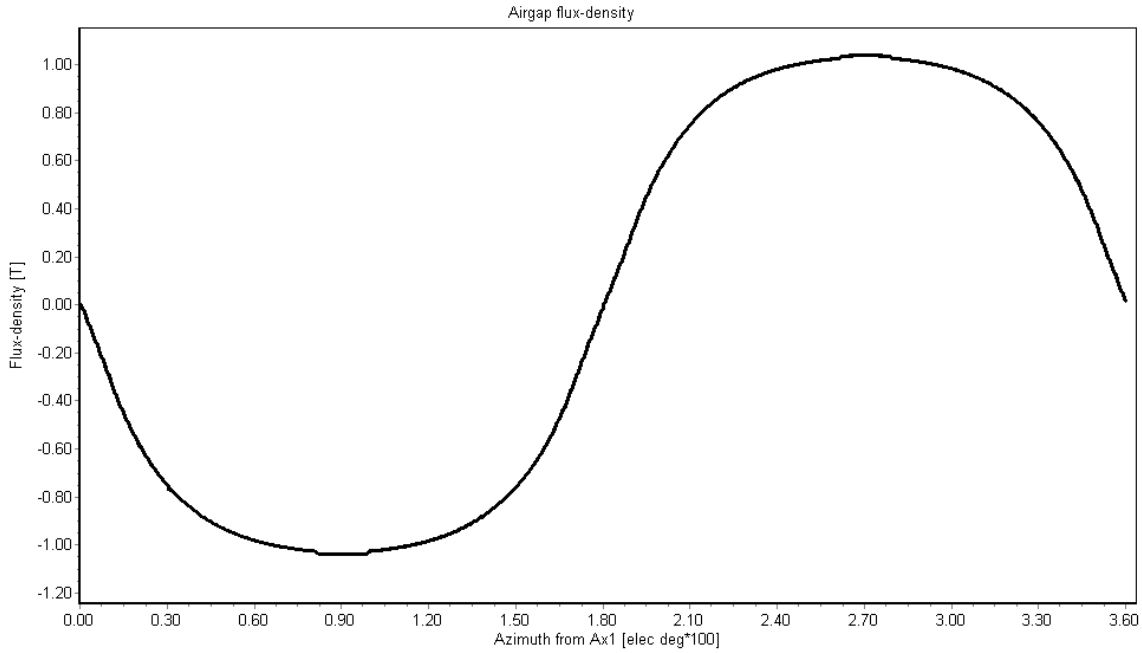

Figure 6.9: Airgap flux density of 24/20 motor

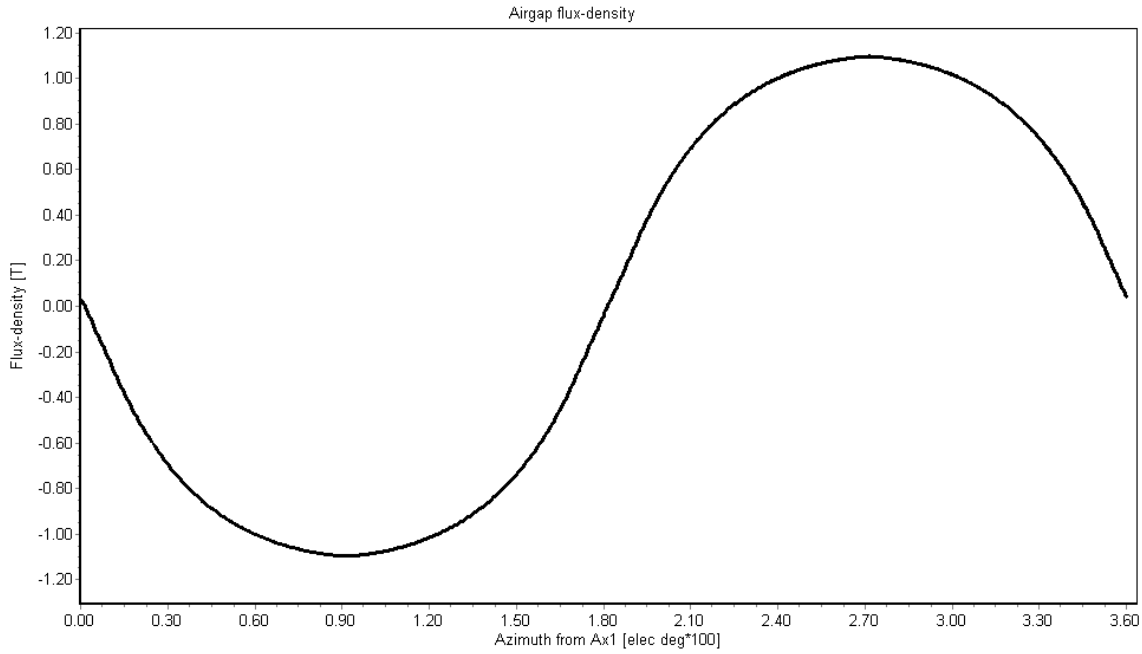

Figure 6.10: Airgap flux density of 24/28 motor

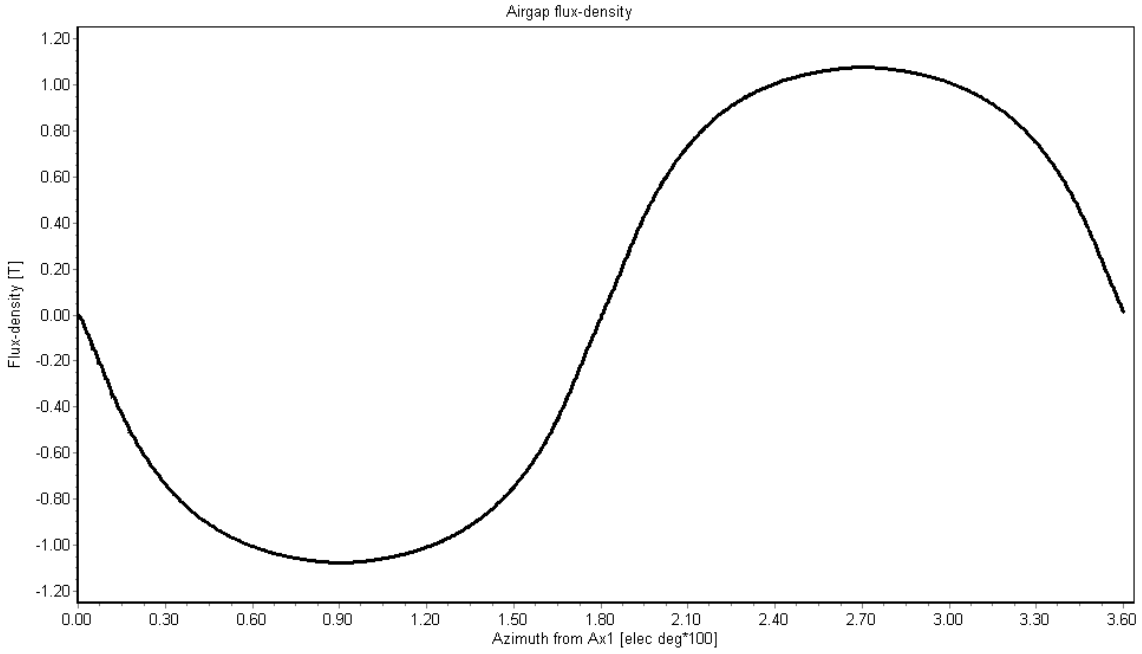

Figure 6.11: Airgap flux density of 36/24 motor

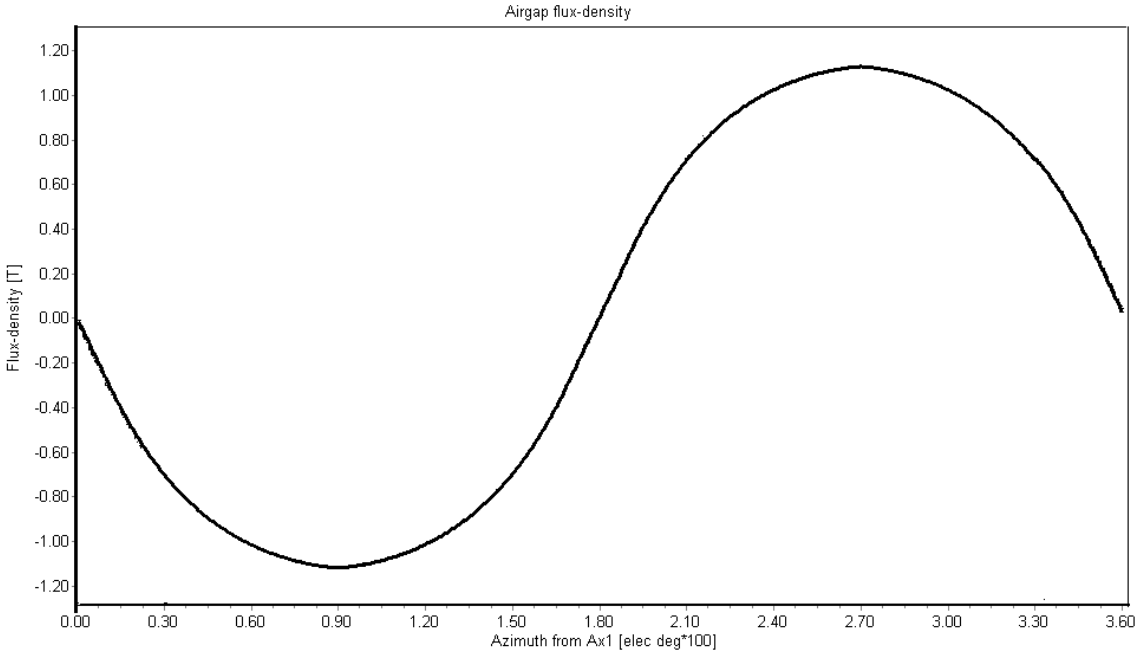

Figure 6.12: Airgap flux density of 48/32 motor

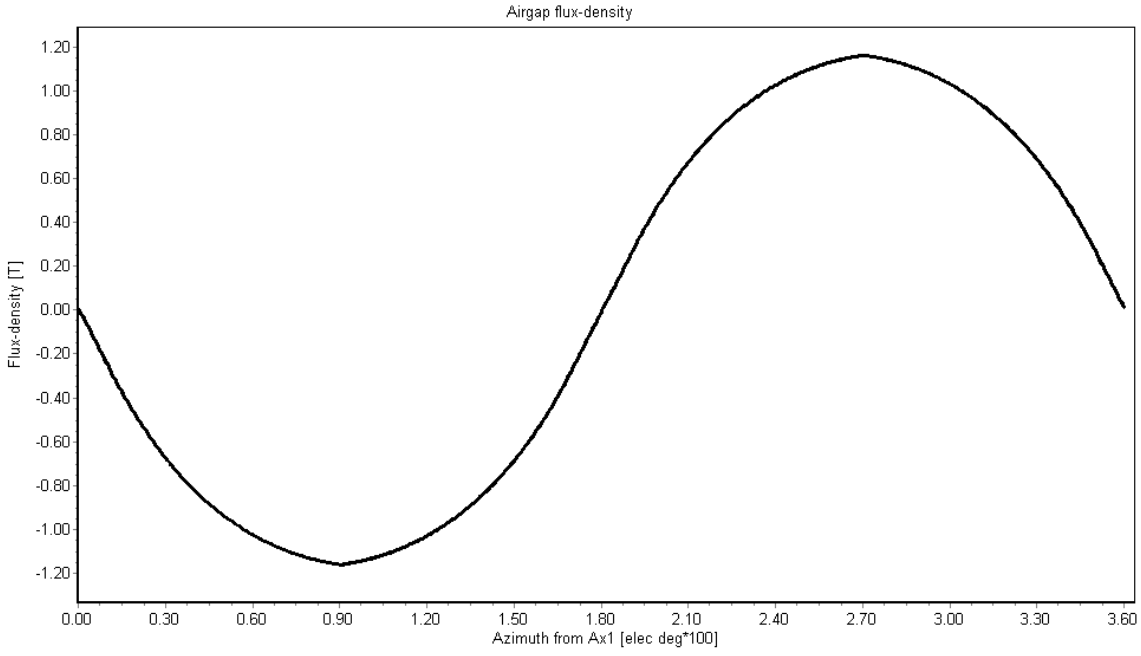

Figure 6.13: Airgap flux density of 48/40 motor

From the airgap flux density plots shown in figures 6.8 to 6.13 it can be seen that as the pole number increase the shape of the plot is becoming more and more sinusoidal. Which is the indication of reduction of harmonics. The harmonic analysis is carried out with the motor design software. Harmonic graphs of the motors are shown in the figures 6.14 to 6.19. The values of the %THD of the motors are obtained.

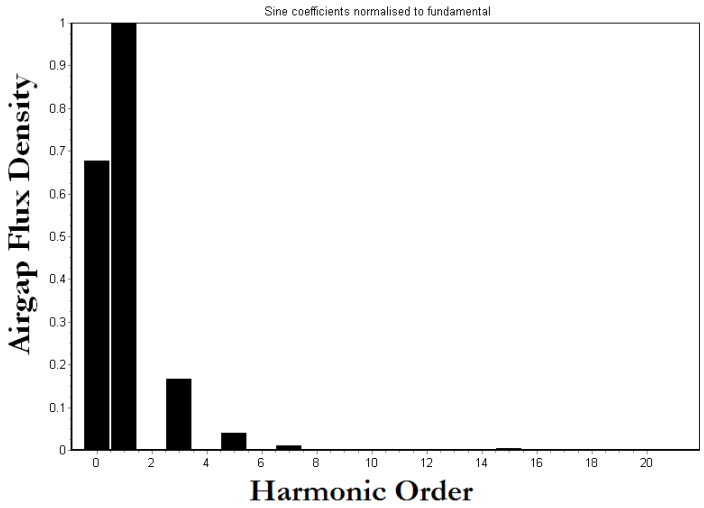

Figure 6.14: Airgap flux density harmonic plot of 24/16 motor

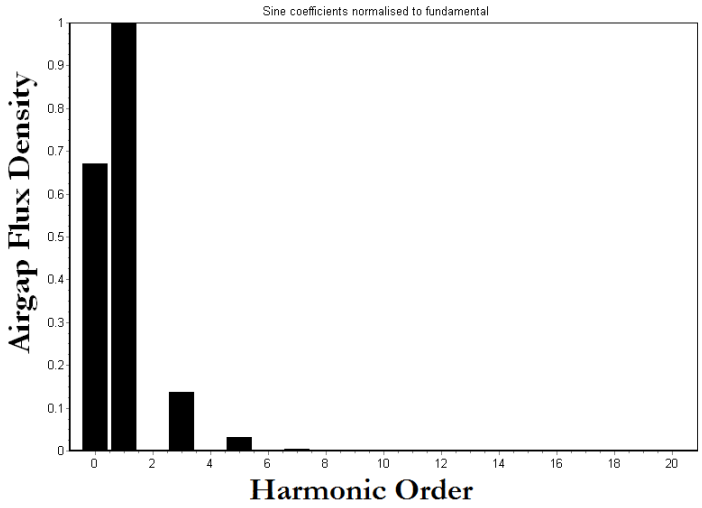

Figure 6.15: Airgap flux density harmonic plot of 24/20 motor

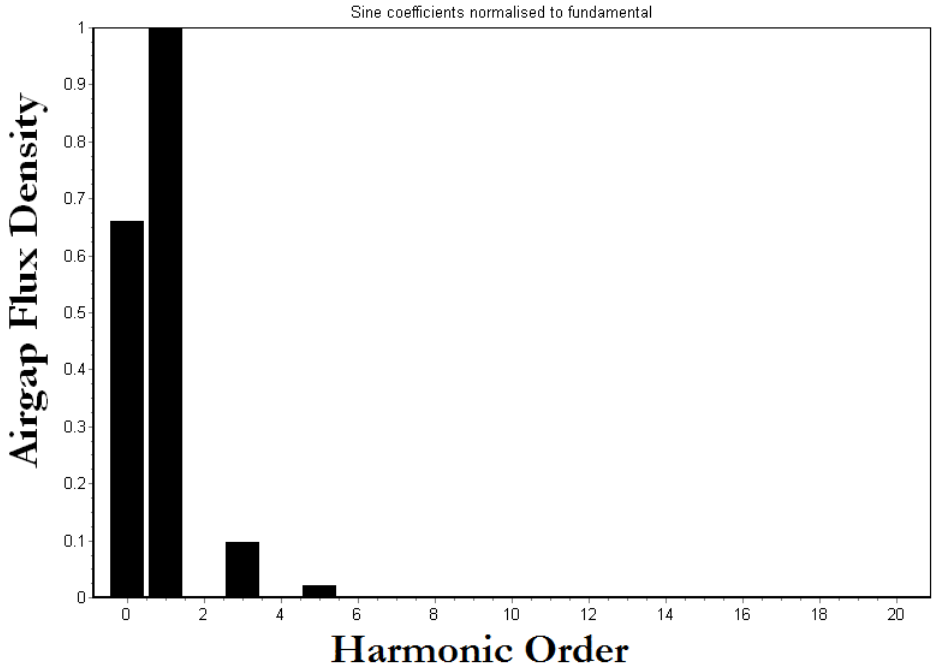

Figure 6.16: Airgap flux density harmonic plot of 24/28 motor

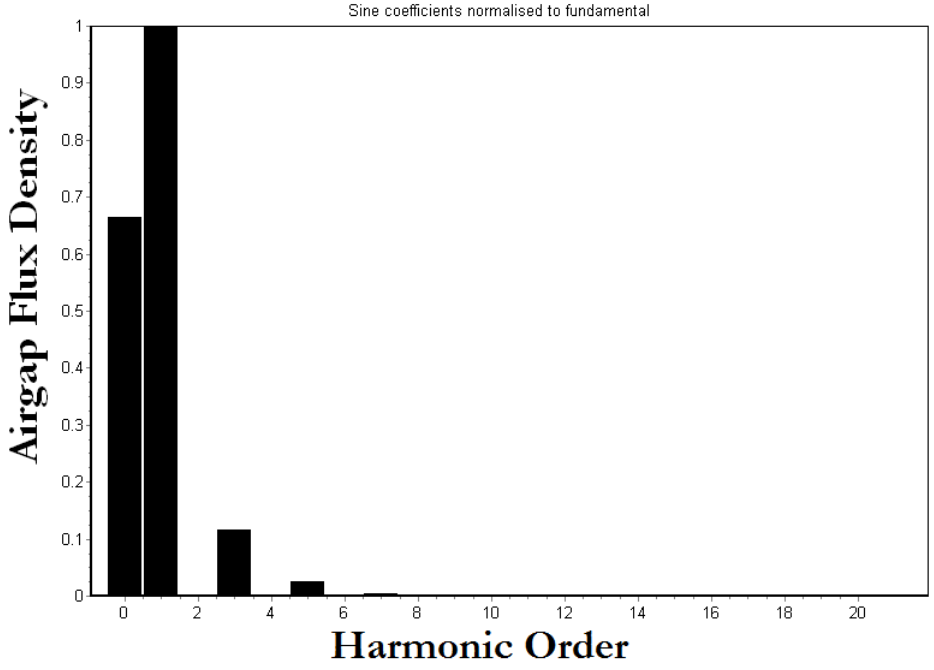

Figure 6.17: Airgap flux density harmonic plot of 36/24 motor

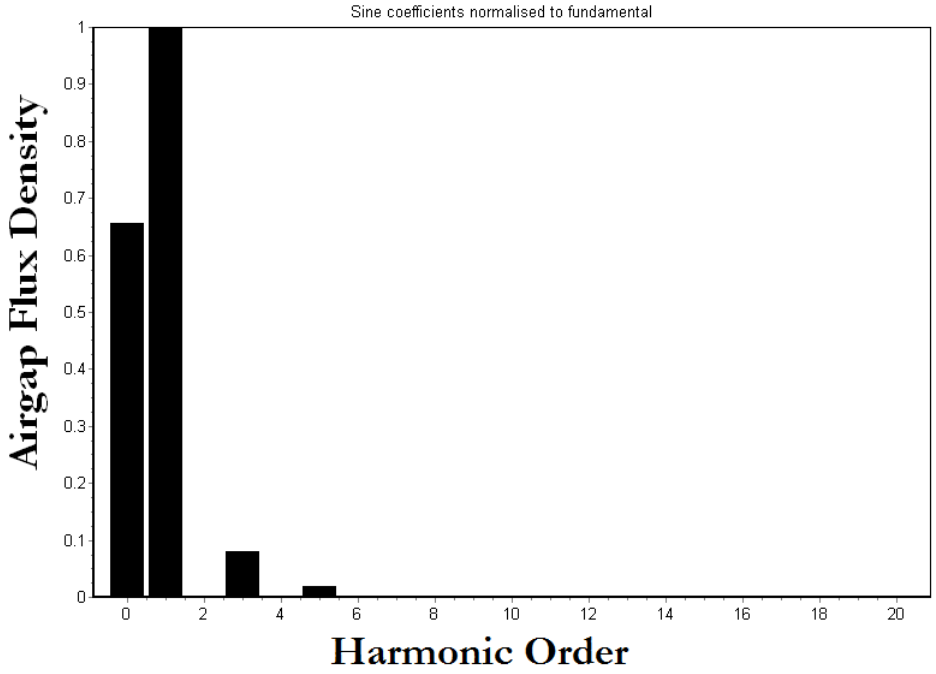

Figure 6.18: Airgap flux density harmonic plot of 48/32 motor

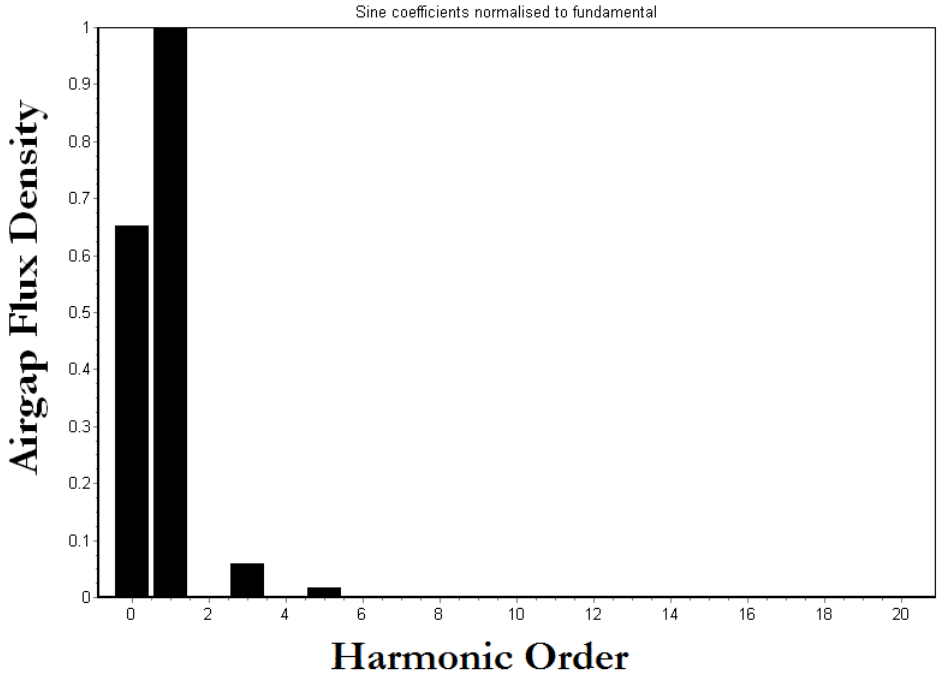

Figure 6.19: Airgap flux density harmonic plot of 48/40 motor

The value of %THD of airgap flux density should be limited to 1%. The values of %THD for the airgap flux density of the designed motors are given in the Table:6.1. The comparative analysis of motors are shown in fig. 6.20.

Table 6.1: % THD of the airgap flux density

Parameter/Motor	M1	M2	M3	M4	M5	M6
%THD of airgap flux density	17.24	14.14	9.87	11.80	8.33	6.08

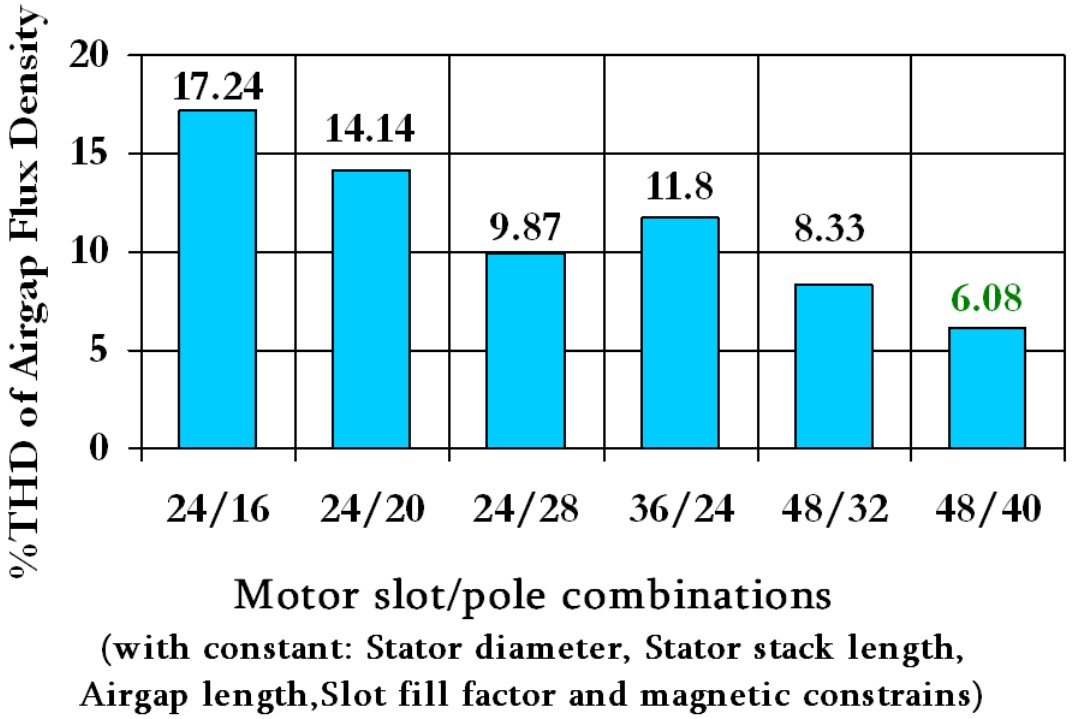

Figure 6.20: Comparison of airgap flux density %THD

From the above results it can be seen that as the number of pole increases for the same number of slots the %THD in the airgap flux density is reduced. As the number of pole is increased the variation in the airgap flux density is reduced and it becomes more and more sinusoidal. The lowest %THD is reported in the motor M6 with slot/pole combination 48/40.

6.3 Choice of design

From the harmonic analysis %THD of no load airgap flux density is obtained. It is observed that from Fig.6.20 the harmonic content is less in the motor M6 (48/40 slot/pole combinations) of Table 6.1. The motor M6 is selected for Finite Element Analysis (FEA). Further reduction of airgap flux density harmonics is carried out with optimization of slot opening width and shaping of PM using FEA.

Chapter 7

Finite Element Analysis

7.1 Basics of FEA

The finite element analysis (FEA) is a numerical technique for finding approximate solutions of partial differential equations (PDE) as well as of integral equations [23]. The Finite Element Method is a good choice for solving partial differential equations over complicated domains, when the domain changes, when the desired precision varies over the entire domain, or when the solution lacks smoothness.

The finite element method is essentially based on subdivision the whole domain in a fixed number of sub-domains. Because of small dimensions of these domains, the function is approximated by simple interpolating functions whose coefficients are unknown quantities. The solution of the field problem is obtained when these unknown coefficients are found. The finite element analysis is organized in following steps:

a. Partition of the domain

b. Choice of interpolating function

c. Formulation of the system to resolve the field problem

d. Solution of the problem

Modern finite element packages use advanced graphical displays which are usually menu-driven to make the process of solving problems as easy as possible. All packages have three main components:

- Pre-processor
- Solver
- Post-processor

Pre-processor is a module where the finite element model is created by the user. This module allows new models to be created and old models to be altered. The different parts of any finite element model are:

- **Drawing:** Drawing the geometric outline of the model using graphical drawing tools.
- **Material:** The different regions of the geometry model are assigned magnetic material properties. The materials can have linear or nonlinear magnetic characteristics. Materials can be defined by their different properties like conductivity, permeability, flux density, coercive force etc.
- **Electric circuits:** Regions which contain coils are linked to current or voltage sources. Specifying the number of turns per coil and the current magnitude.
- **Constrains:** The edges of the model usually need constraints and this is done by defining constraints graphically.

Solver module solves numerically the field equations. The pre-processor module sets which solver (electrostatic, magnetostatic, eddy-current) should be used. Mostly, adaptive meshing is implemented to ensure efficient mesh discretization. The solver starts by creating a coarse finite element mesh and solving it. An error estimate is produced from this solution, and the mesh is refined and solved again. This is repeated until the mesh is refined sufficiently to produce an accurate result.

Post-processor is an interactive module that displays field quantities such as magnetic vector potential, flux density, field intensity and permeability. It also gives the user access to a vast amount of information regarding the finite element solution such as energy, force, torque and inductance, which are all built into the module.

In this study the finite element software used is MAGNET. Magnet Solver Capabilities:

- Static magnetic fields in and around specified DC current distributions and permanent magnets
- AC magnetic fields and phase differences caused by eddy currents in and around sinusoidal current-carrying conductors at a single frequency in the complex domain
- Time-varying magnetic fields and time lag effects caused by induced eddy-currents in and around current-carrying conductors and permanent magnets
- The effects of motion: multiple components in linear, rotational or arbitrary directions.

7.2 FEA simulation

PMSM with different slot/pole combinations is analyzed for airgap flux density harmonics in the previous section. Analytic design of selected motor with 48/40 slot/pole combination is now verified with the FEA. The ratings of the motor for the analysis purpose are as follows:

- Rated Power : 45 kW
- Rated Speed : 400 rpm
- Rated Torque : 1000 Nm

7.2.1 Creating FE model

The finite element modeling has several properties which has to be assigned properly to the geometry of the model. The geometric model of the motor is drawn as per mentioned dimensions in Table 7.1.

Table 7.1: Geometry parameters

Sr. No.	**Parameter**	**Symbol**	**Value**	**Unit**
1	Poles	p	40	–
2	Slots	Q_s	48	–
3	Outer stator diameter	D_o	400	mm
4	Inner stator diameter	D	282	mm
5	Outer rotor diameter	D_{rc}	220	mm
6	Stator stack length	L	140	mm
7	Airgap length	δ	1	mm
8	Stator slot height	h_{ss}	50	mm
9	Stator slot opening	b_{so}	5	mm
10	Magnet thickness	h_m	30	mm

The cross section view of 48/40 PMSM is shown in fig. 7.1.

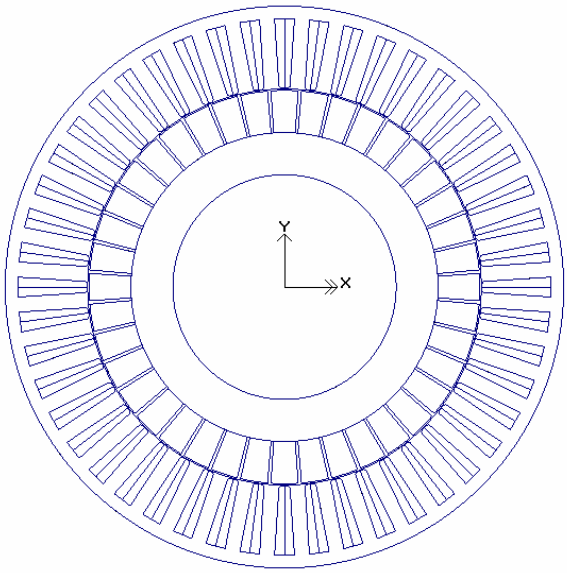

Figure 7.1: Cross section view of 48/40 PMSM

The magnetic material are assigned to the different parts of the motor. Conducting material is assigned to the conductors. All the electrical and magnetic properties are defined. Then coil at each and every conductor of slot is made. According to winding diagram these coils are connected with each other and the polarity is checked. Coils are then fed with the sinusoidal currents each 120 degree apart. The 2D and 3D model of the PMSM after the modeling is completed is shown in fig. 7.2 and fig. 7.3 respectively.

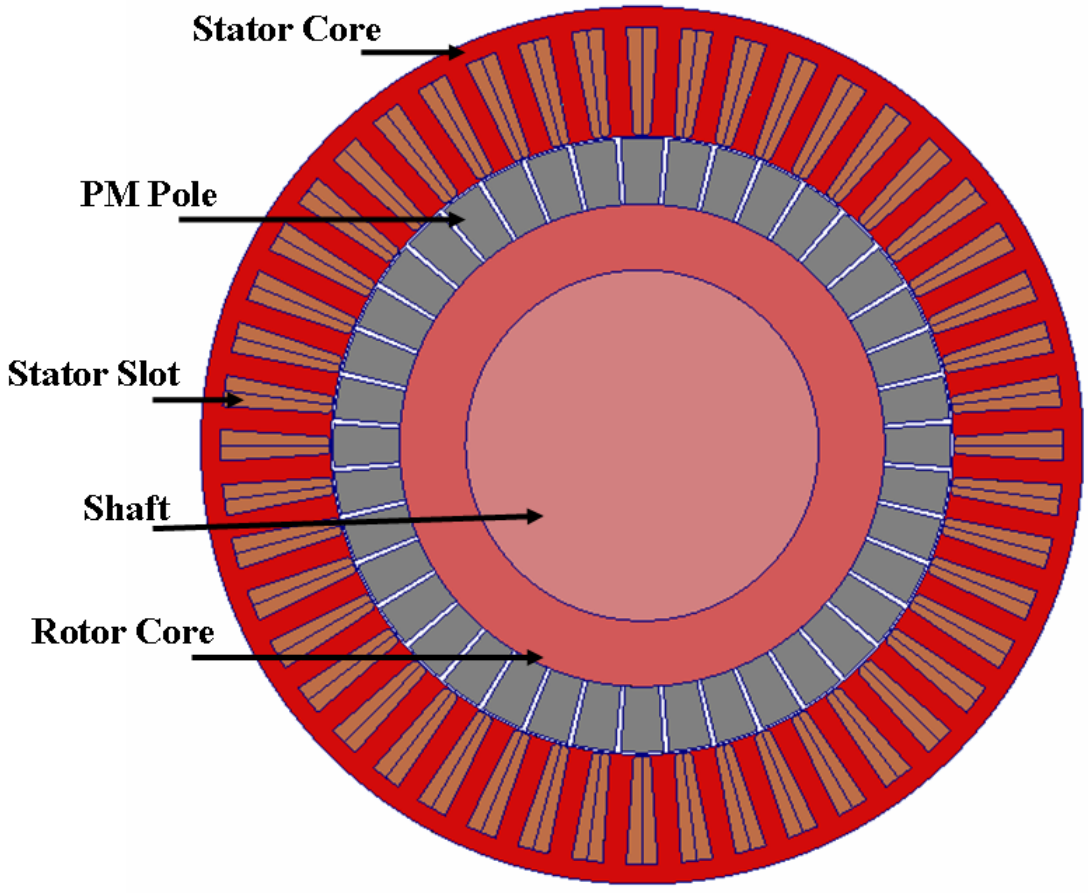

Figure 7.2: 2D FE model of 48/40 PMSM

2D mesh generation and refinement of the mesh then carried out. Whenever a mesh is generated, it is important to consider the requirements of different regions. A fine mesh produces higher accuracy but it takes more time to solve the model. So the

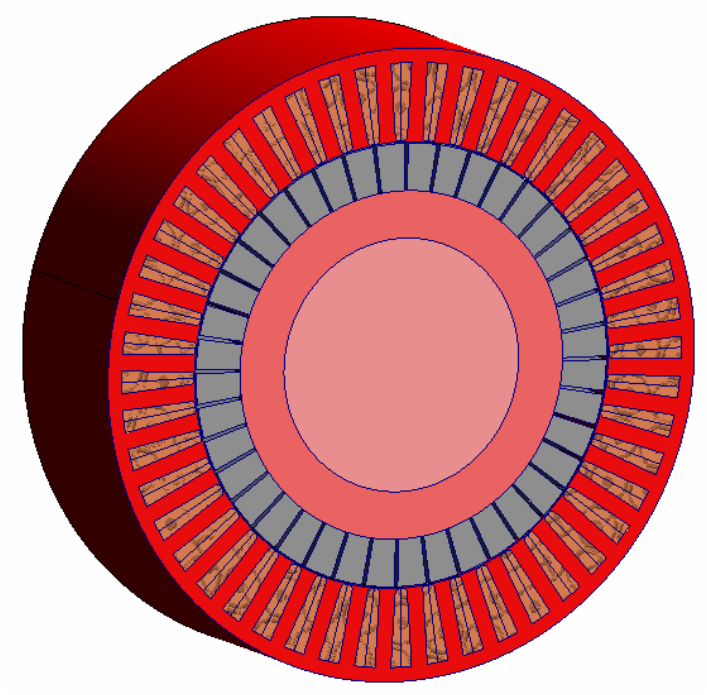

Figure 7.3: 3D FE model of 48/40 PMSM

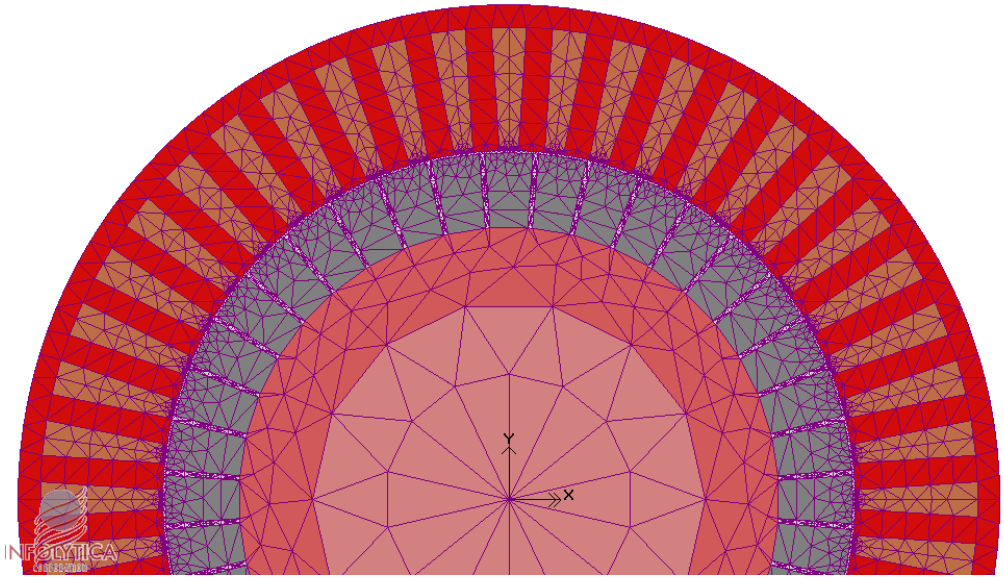

Figure 7.4: Meshing of PMSM model

regions in which higher accuracy is needed only should be having fine mesh. The air-gap region in the model is refined with fine mesh. Which produces higher accuracy in airgap flux density and torque calculations. The automatic mesh generator produces

adequate mesh in terms of quality, accuracy and size. However it is better to adjust and control the density of the mesh with a specific region. The generated mesh with refinement is shown in fig. 7.4.

After model is created the Static and Transient analysis is performed on the model. The values of flux density in the teeth, stator core, rotor core and airgap is analyzed and verified with the analytic design of the motor as assumed in chapter 5. The torque plot is also obtained after the analysis.

7.2.2 FEA simulation results

Static analysis results are shown by the flux contour plot, flux density plot, arrow plot and different values of the parameters. The flux plot is shown in the fig. 7.5. Flux path is shown by the flux plot.

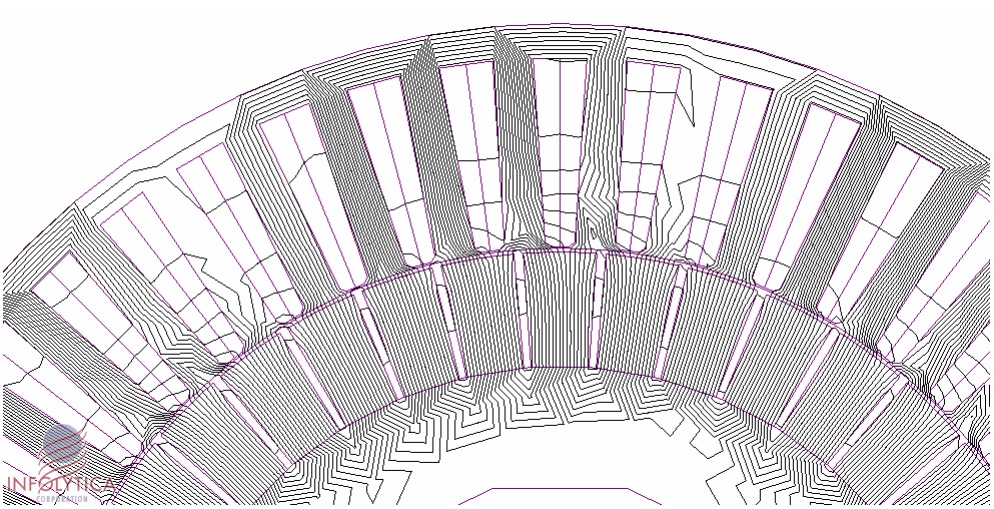

Figure 7.5: Flux contour plot (Magnified View)

The flux density at different part of the motor after the excitation of the winding is shown by the flux density plot as shown in fig. 7.7. The flux density at teeth, stator core and rotor core is analyzed. The values of these flux densities are matched with the analytic design of the motor.

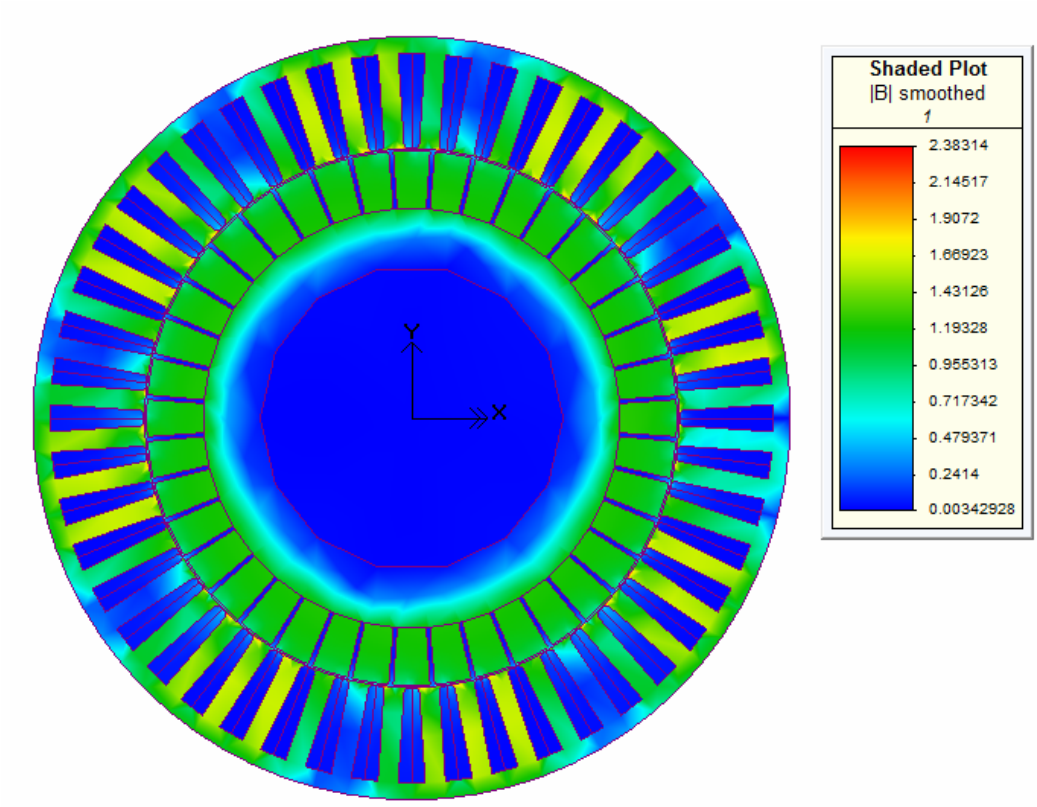

Figure 7.6: Flux density plot

Table 7.2: Flux density comparison

Flux density	**Analytic Values**	**FEM Values**
B_{st}	1.6937	1.6692
B_{sy}	1.0861	1.1367

All the values of flux density are approximately same with the analytic design as shown in Table 7.2. The flux density in stator teeth and stator core is compared to the expected design values.

Arrow plot of the flux density is shown in the fig. 7.8, which shows the direction of the flux inward or outward from the magnet.

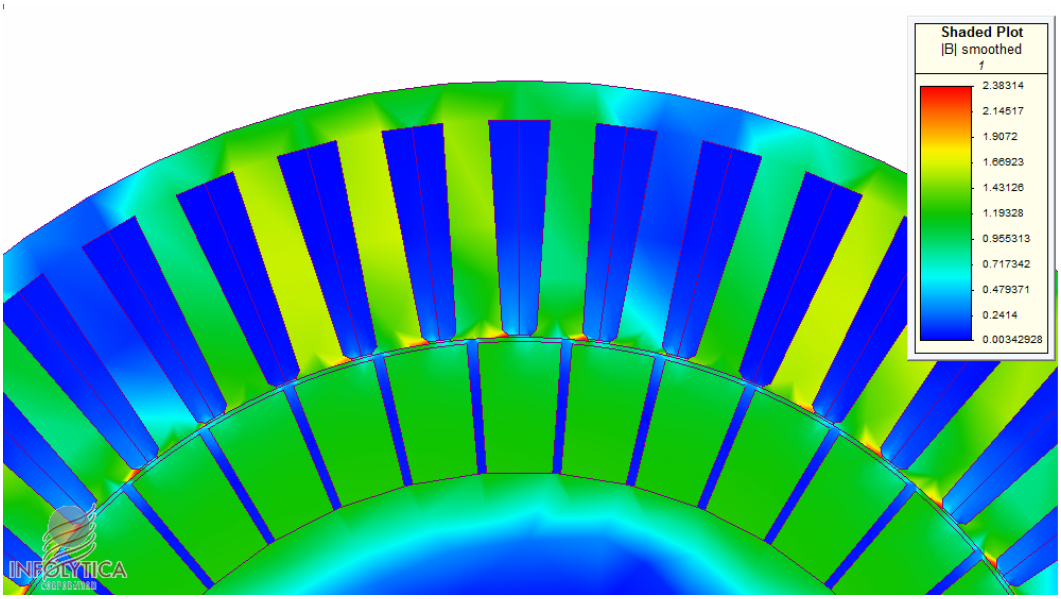

Figure 7.7: Flux density plot (Magnified View)

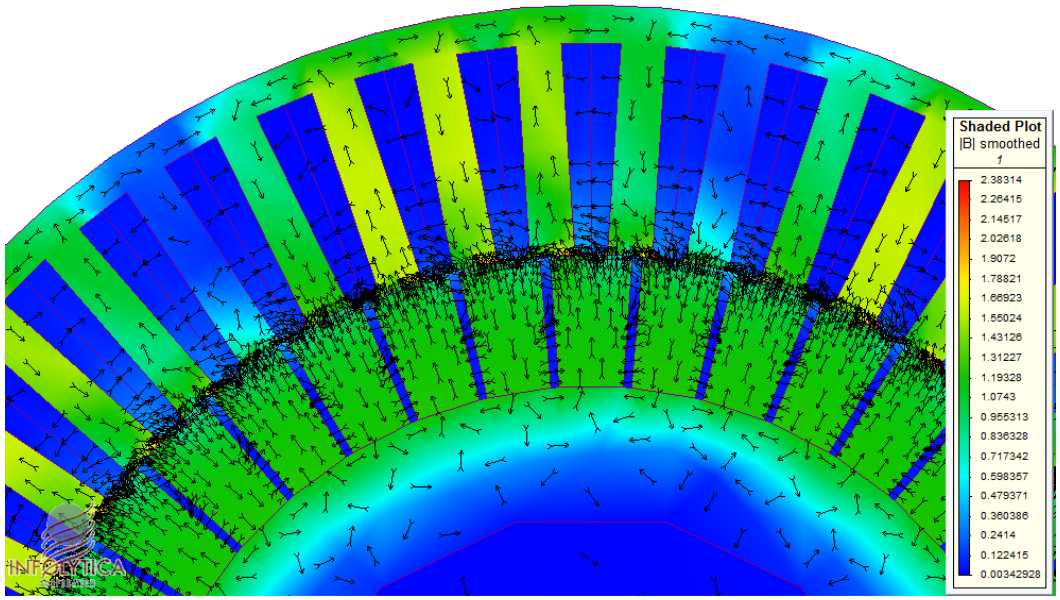

Figure 7.8: Flux density arrow plot

Instantaneous magnetic energy and co-energy plot are also obtained which are help full for the torque and inductance calculations for the analysis purpose. Fig. 7.9 and fig. 7.10 shows the instantaneous magnetic stored energy and co-energy plot respectively.

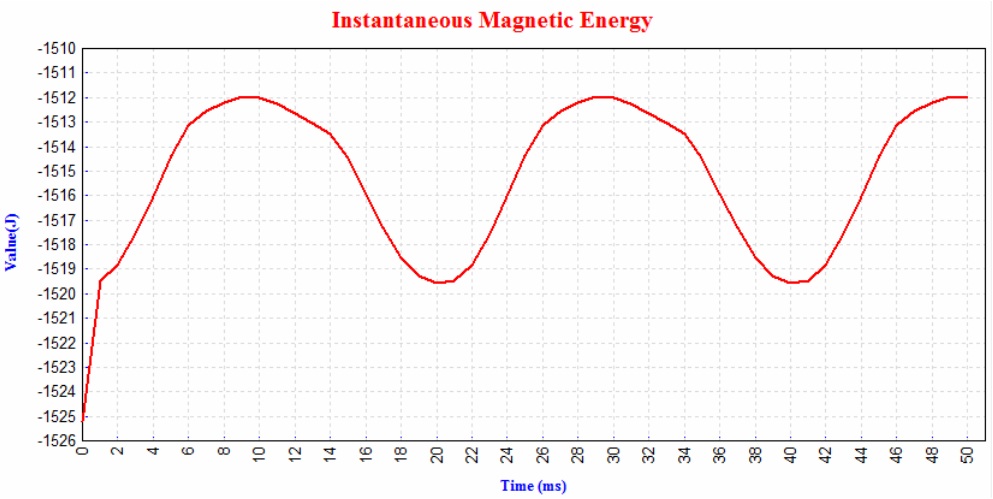

Figure 7.9: Instantaneous magnetic energy

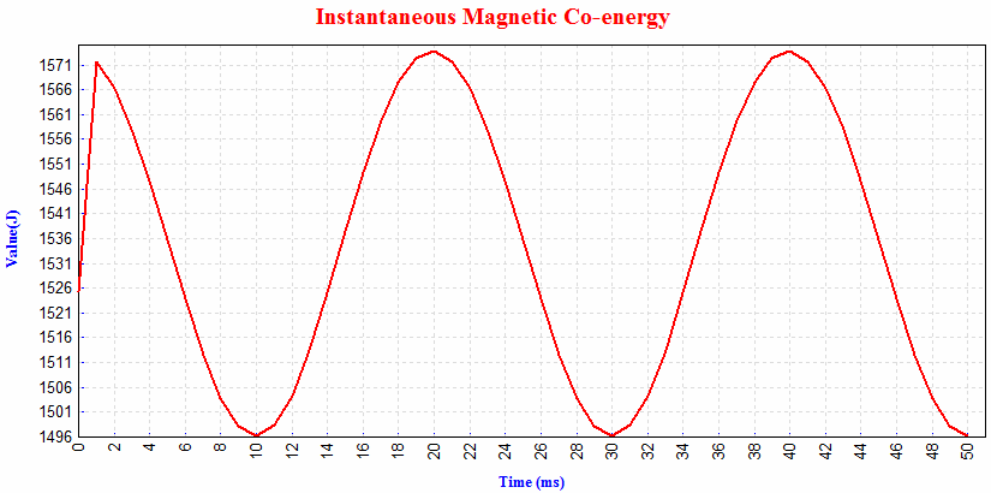

Figure 7.10: Instantaneous magnetic co-energy

The transient analysis is then carried out after static 2D analysis. In transient analysis time step is to be decided and the configured in the solver options. The transient analysis gives the different values at each time step selected. The graph of the torque about origin v/s time is obtained as shown in fig. 7.11.

Value of torque obtained from the static 2D analysis is 958.87 Nm which is 4.113% less than the analytic value of 1000 Nm. The torque with respect to rotor position is

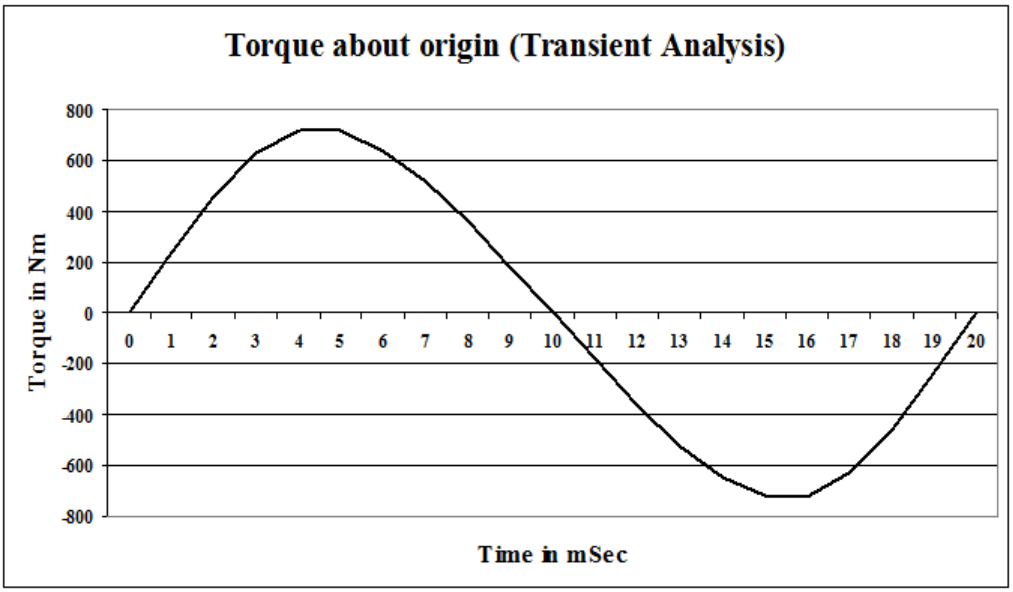

Figure 7.11: Torque about origin (Transient Analysis)

found. At each rotor position in mechanical degree the value of torque is found. The graph of Torque v/s Rotor position is plotted as shown in fig. 7.12.

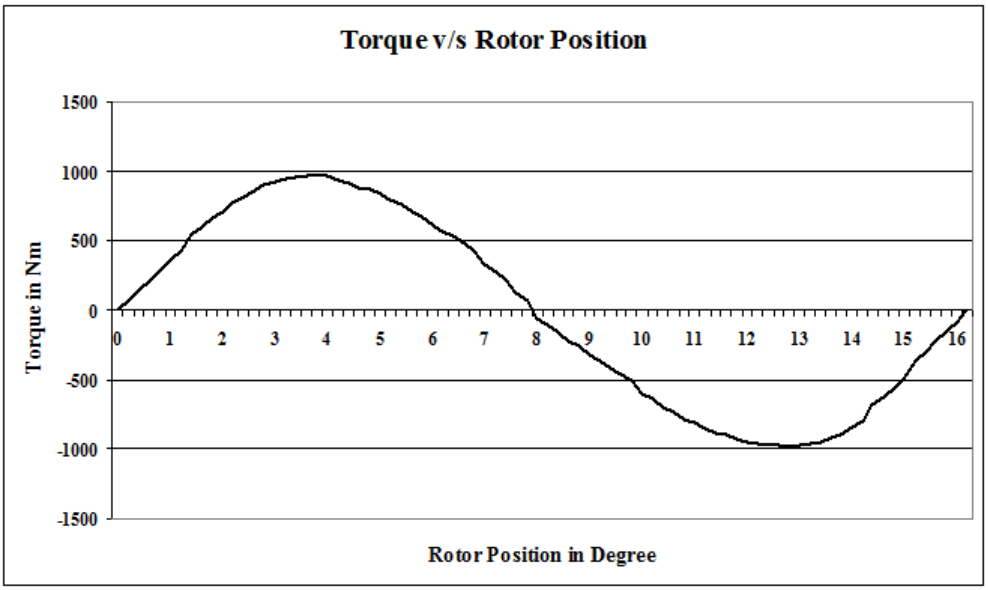

Figure 7.12: Torque v/s Rotor position

Chapter 8

Harmonics in PMSM

The main drawback of the PMSM with fractional slot concentrated winding is the production of harmonics which increases the vibrations and causes extra heating to the motor. PMSMs with different slot/pole combinations is designed and analyzed with concentrated windings. In this section the harmonics analysis is performed with the help of finite element analysis. Then the optimization of the airgap flux density is carried out with the change in the design of the selected motor.

8.1 Harmonic calculation

Airgap flux density at each rotor position is measured and the plot of Airgap flux density v/s Rotor position is obtained. The waveform of airgap flux density is analyzed and the harmonic plot is obtained. The % THD of the airgap flux density is calculated from the harmonic plot with the help of computer program. The airgap flux density waveform is shown in fig. 8.1 and FFT is shown in fig. 8.2. From the FFT plot the %THD calculated is 34.73%. The measures to reduce this %THD is taken by the optimization procedure.

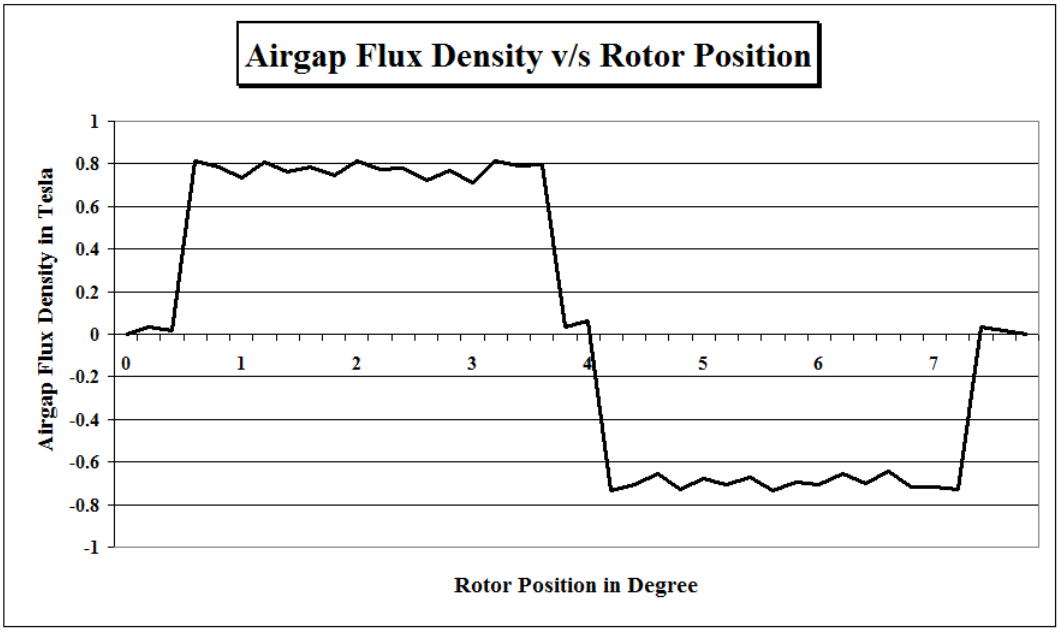

Figure 8.1: Airgap flux density

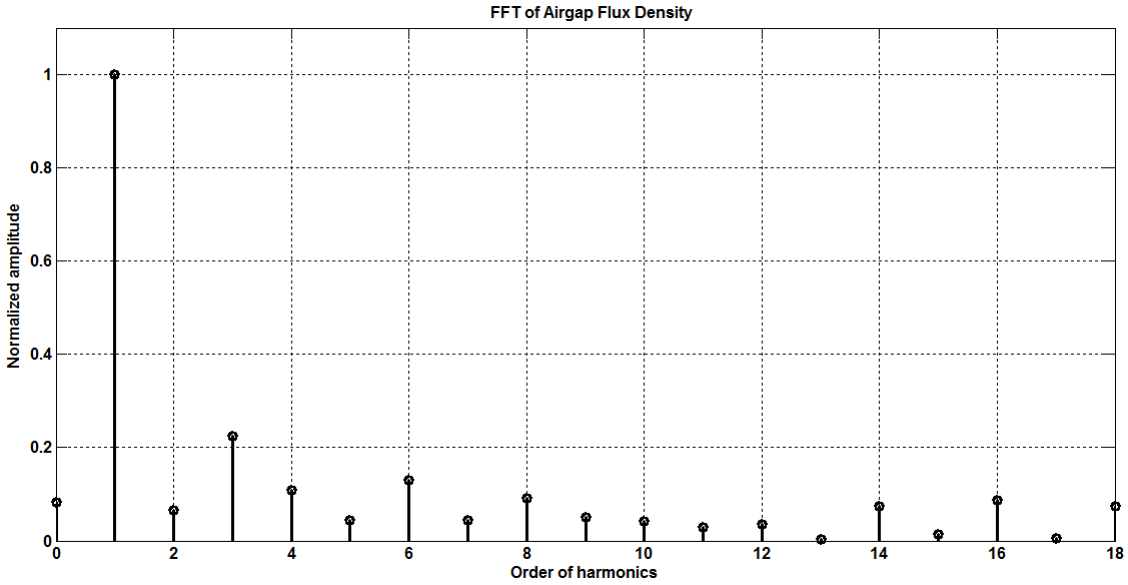

Figure 8.2: FFT of Airgap flux density

8.2 Harmonic reduction technique

8.2.1 Varying stator slot opening width

The airgap flux density can be optimized by varying the stator slot opening width. With wider slot opening the permeance variation in the airgap is more. To reduce the permeance variation narrow slot opening width is used. The stator slot opening width is changed from 5mm to 1mm and the airgap flux density waveform is analyzed. Fig. 8.5 shows the airgap flux density waveform with 1mm slot opening width. The FFT plot is shown in fig.**??**.

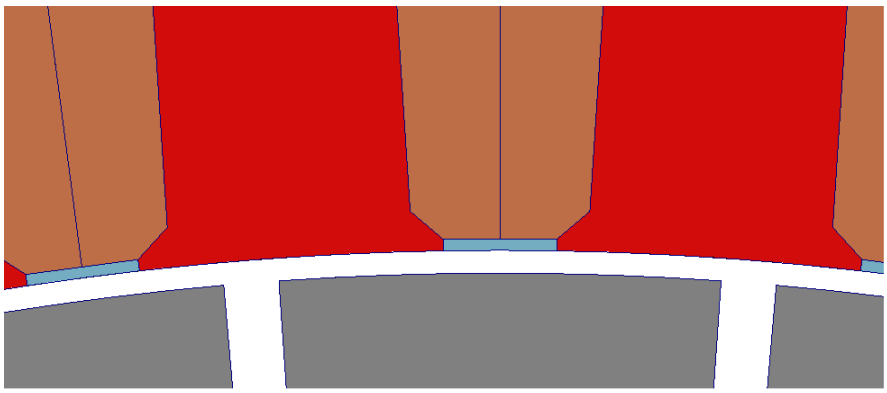

Figure 8.3: Slot opening width with 5mm

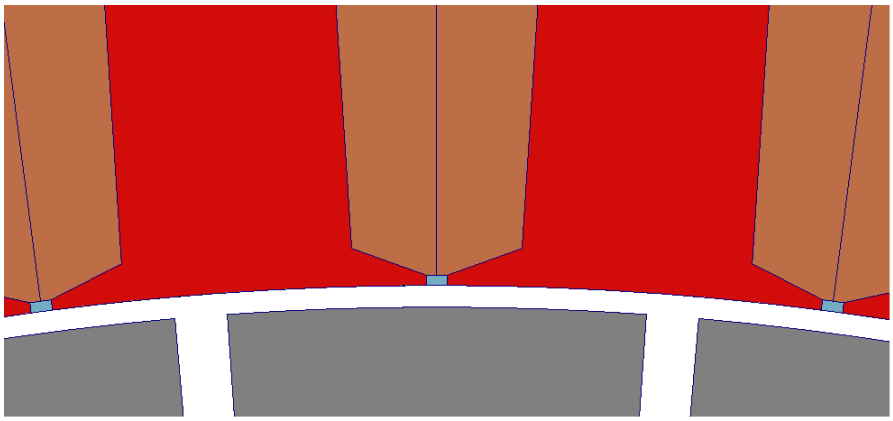

Figure 8.4: Slot opening width with 1mm

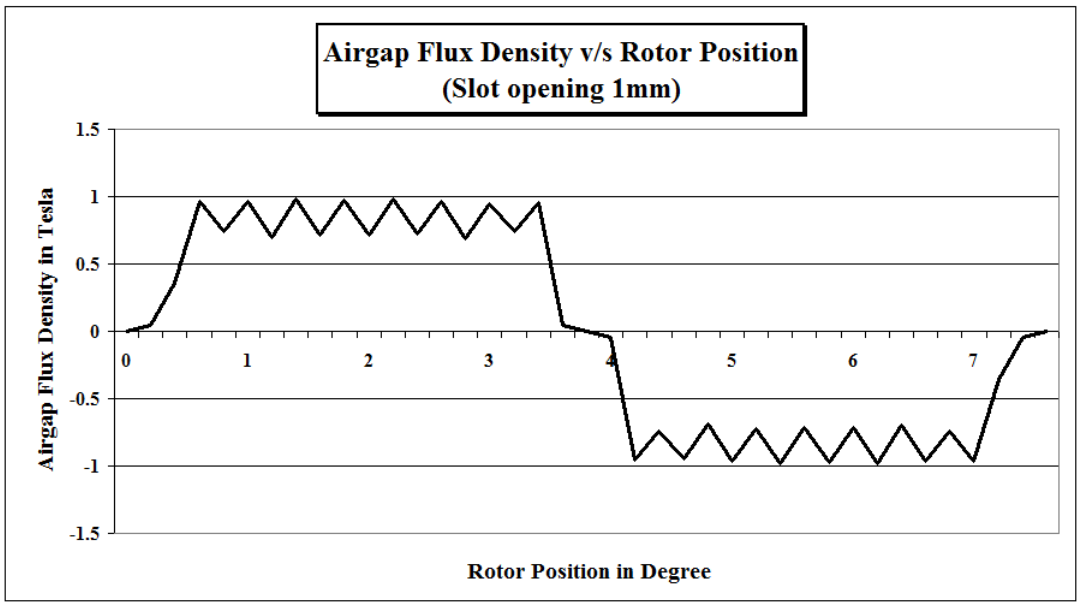

Figure 8.5: Airgap flux density with slot opening 1mm

8.2.2 Shaping of permanent magnet

The airgap flux density depends upon the shape of magnets. As the shape of magnet changes waveform of airgap flux density changes significantly. By selecting proper shape of magnet specific space harmonics can be eliminate and the airgap flux density quality and the motor operation performance can be increased.

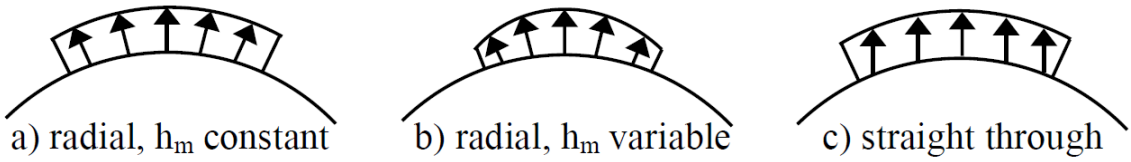

Figure 8.6: Magnet shape and magnetization

Fig. ?? shows the three different magnet shapes and magnetization. On the left side, the radially magnetized magnets have a constant height h_m. In the middle, the magnet shape is adjusted to give a more sinusoidal flux distribution in the airgap. A

common solution is to cut the edges of the magnets to soften the flux distribution. In return, there is a higher risk of demagnetization at the thin parts of the magnets (the magnet height h_m should be bigger than 2-2.5 mm for manufacturing). The straight through magnetization shown in fig. 8.6c is another possibility to get a more sinusoidal field.

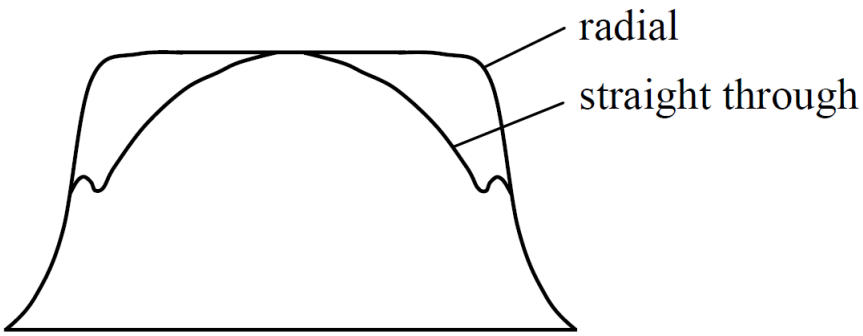

Figure 8.7: Airgap flux for different magnetization

Fig. 8.7 shows the airgap flux distribution for radial and straight through magnetization. The biggest disadvantage of the straight through magnetization is the lower peak value of the first harmonic of the flux density (compared to radial magnetization) that must be compensated with more magnet material.

By changing the magnet pole shape the airgap flux density shape is changed as shown in fig. 8.7. With the use of Bread Loaf type magnet shape airgap flux density becomes sinusoidal. The Bread Loaf type magnet shape is shown in fig. 8.9. Fig. 8.10 shows the airgap flux density waveform obtained by changing magnet shape with bread loaf type.

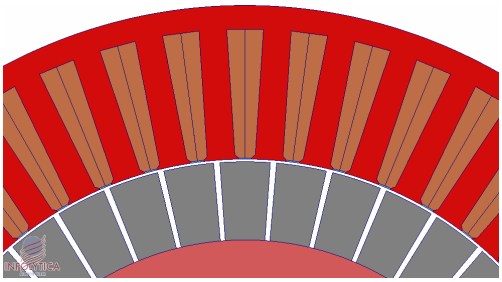

Figure 8.8: Simple magnet shape as main pole

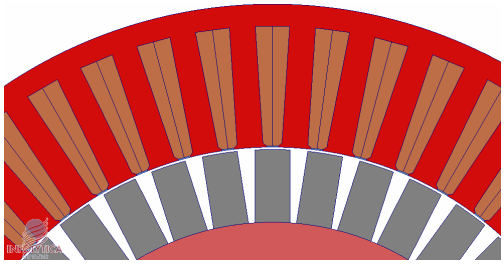

Figure 8.9: Bread loaf type magnet shape as main pole

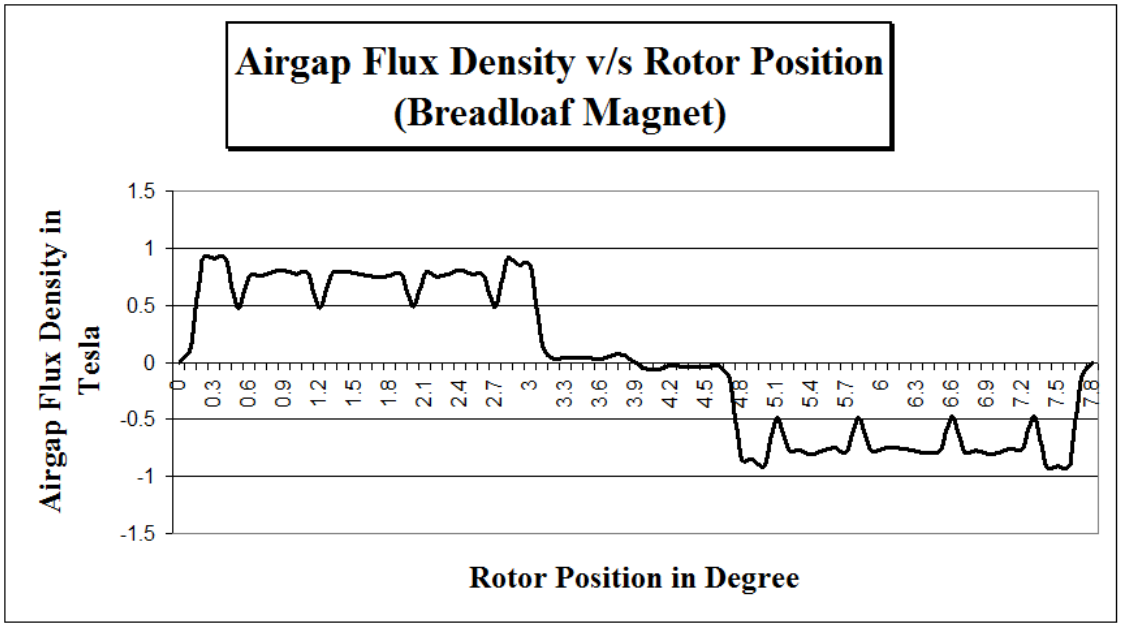

Figure 8.10: Airgap flux density with bread loaf magnet

8.3 Result Comparison

Optimization of the airgap flux density is carried out with Finite Element Analysis. The magnet shape and stator slot opening width is analyzed. The airgap flux density waveforms are obtained and the FFT of these waveforms is calculated with the help of computer program. From the comparison of the harmonics obtained with different techniques we can comment on the airgap flux density. Fig. 8.11 shows the comparison of harmonics of airgap flux density.

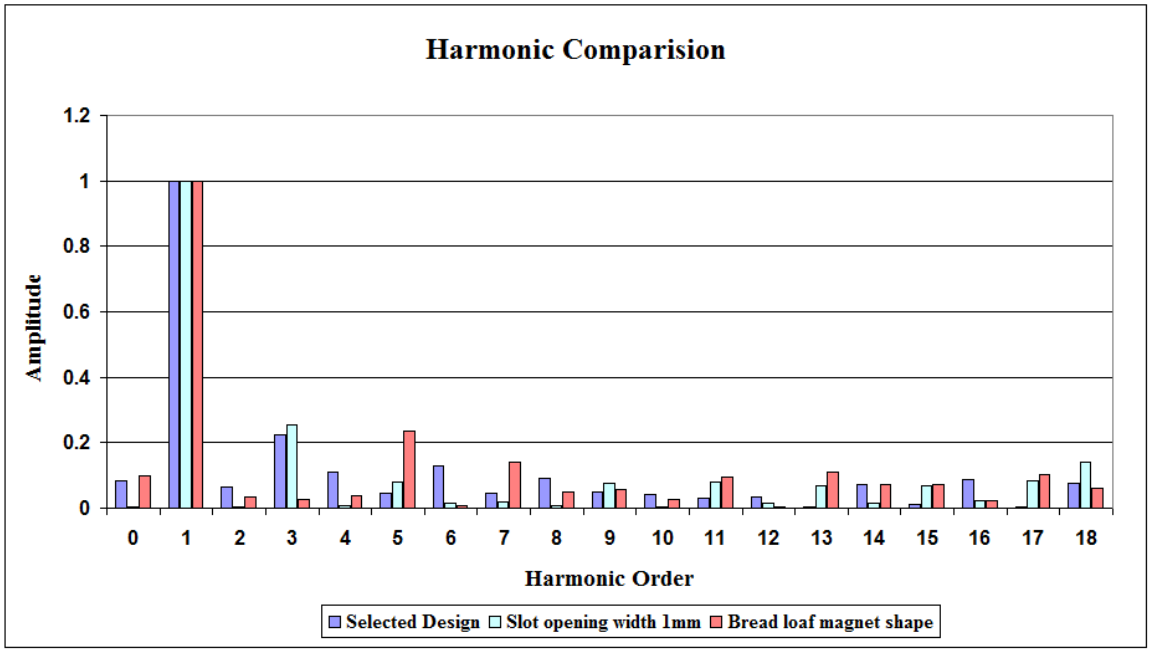

Figure 8.11: Comparison of FFT of airgap flux density

With the Bread loaf type of magnet shape the 3^{rd} harmonic is reduced significantly, but 5^{th} and 7^{th} harmonics are increasing. Here it can be seen that with bread loaf type magnet all the tripplen harmonics are reducing in magnitude. By decreasing the stator slot opening width from 5 mm to 1 mm, the value of 5^{th} and 7^{th} harmonics are reduced while 3^{rd} harmonic amplitude is increasing. By proper shaping and slot opening width airgap flux density harmonics can be reduced by optimizing the shape of the flux density waveform.

Chapter 9

Conclusion and Future Scope

9.1 Conclusion

The low speed direct drive motors are more advantageous against induction motors as it requires less maintenance and more efficient. For low speed direct drive applications fractional slot concentrated winding found advantageous compared to conventional integer slot distributed winding. The merits and demerits of the fractional slot concentrated winding are presented. In this study the motors are designed with fractional slot concentrated winding.

Analytical design of PMSM is shown. The main drawback of the PMSM with fractional slot concentrated winding is the production of harmonics in the airgap flux density, which increases the vibrations and causes extra heating to the motor. To reduced the harmonics in airgap flux density different motors with various slot/pole combinations are designed and compared for harmonic content in the airgap flux density. The motors are designed with motor design software. Motor specifications are 45 kW, 400 rpm and with the rated torque of 1000 Nm used for the Pulp and Paper industry applications.

Analytical equations of the airgap flux density harmonics are shown. From the harmonic analysis performed with the motor design software with different motors it is observed that as the number of pole increases the harmonic content is decreases for the same slot number. It is also reported that the %THD in the airgap flux density is lowest in the motor with 48/40 slot/pole combination. The total harmonic distortion reported in the motor M6 is 6.08%. The motor with 48/40 slot/pole combinations gives better results than the other motors. PMSM with 48/40 slot/pole combination is selected.

This project work resulted in a selection of particular machine design. This selected design is further studied with finite element method (FEM) in order to verify the analytical results. A comparison is made between analytical design and FEM simulation, the result shows acceptable correlation, leading to the fulfillments of the requirements.

Further optimization of the design to reduce airgap flux density harmonics is carried out with the FEM simulations. The shaping of permanent magnet and varying the stator slot opening width, the optimization is obtained.

9.2 Future scope

The further reduction of harmonics of the motor can be carried out by different winding configurations. Proper shaping of PM flux density waveform can further optimized to sinusoidal. By varying the magnet width some particular harmonics can be eliminated.

References

[1] Jerome Cros and Philippe Viarouge, "Synthesis of High Performance PM Motors with Concentrated Windings", IEEE Transactions on Energy Conversion, Vol. 17, NO. 2, pp. 248-253, June 2002.

[2] Pia Salminen, Markku Niemel, Juha Pyrhnen and Juhani Mantere, "Performance analysis of fractional slot wound PM-motors for low speed applications", IAS 2004, 0-7803-8486-5/04/$20.00 ©2004 IEEE, pp. 1032-1037.

[3] Pragasen Pillay, "Application Characteristics of Permanent Magnet Synchronous and Brushless dc Motors for Servo Drives", IEEE Transactions on Industry Applications, Vol. 21, No. 5, pp. 986-996, September/October 1991.

[4] Li Xiao-hai , Zhu Li, Zhao Ji-min, Jiang Shu-zhong, "Research on Special Low-Speed, High-Torque Permanent Magnet Synchronous Motor for Screw Pump", IPEMC2009, 978-1-4244-3557-9/09/$25.00 ©2009 IEEE, pp. 1858-1862.

[5] Xu Yanliang Sun Yuanyuan, "Fractional-slot Low Speed Large Torque Permanent Magnet Brushless Motors", ICIEA 2009, 978-1-4244-2800-7/09/$25.00 ©2009 IEEE, pp.3565-3569.

[6] Pia Marjatta Lindh, Hanne Kaarina Jussila, Markku Niemela, Asko Parviainen, and Juha Pyrhnen, "Comparison of Concentrated Winding Permanent Magnet Motors With Embedded and Surface-Mounted Rotor Magnets", IEEE Transactions on Magnetics, Vol. 45, No. 5, pp. 2085-2089, May 2009.

[7] H. Jussila, P. Salminen, M. Niemela and J.Pyrhonen, "Guidelines for Designing Concentrated Winding Fractional Slot Permanent Magnet Machines", POWERENG 2007, April 12-14, 2007, Setbal, Portugal, 1-4244-0895-4/07/$20.00 ©2007 IEEE, pp. 191-194.

[8] Jian Gao, Yanan Yu, Shoudao Huang, "Winding Layers and Slot/Pole Combination in Fractional Slot/Pole PMSM - Effects on Motor Performance", IEEE Explore.

[9] Ayman M. El-Refaie, and Thomas M. Jahns, "Impact of Winding Layer Number and Magnet Type on Synchronous Surface PM Machines Designed for Wide Constant-Power Range Operation" IEEE Transaction on Energy Conversion, Vol. 23, No. 1, pp. 53-60, March 2008.

[10] J. A. Gemes, A. M. Iraolagoitia, M. P. Donsin, and J. I. Del Hoyo, "Analysis of Torque in Permanent Magnet Synchronous Motors with Fractional Slot Windings", Proceedings of the 2008 International Conference on Electrical Machines, Paper ID 1181, 978-1-4244-1736-0/08/$25.00 ©2008 IEEE, pp.1-4.

[11] G. Sooriyakumar, R. Perryman and S. J. Dodds, "Cogging Torque Analysis for Fractional Slot/Pole Permanent Magnet Synchronous Motors", UPEC 2007, pp. 188-191.

[12] J. H. Walker and N. Kerruish, "Design of Fractional Slot Windings", The Institution of Electrical Engineers, Paper No. 2678 S, pp. 428-440, Aug. 1958.

[13] Mircea Popescu, David G. Dorrell, Dan Ionel and Calum Cossar, "Single and Double Layer Windings in Fractional Slot-per-Pole PM Machines - Effects on Motor Performance", 978-1-4244-1-1766-7/08/$25.00 ©2008 IEEE, pp. 2055-2060.

[14] Nicola Bianchi, Silverio Bolognani, and Michele Dai Pr, "Magnetic Loading of Fractional-Slot Three-Phase PM Motors With Nonoverlapped Coils", IEEE

Transactions on Industry Applications, Vol. 44, No. 5, pp. 1513-1521, September/October 2008.

[15] P. Salminen, M. Niemel, J. Pyrhnen and J. Mantere, "High-Torque Low-Torque-Ripple Fractional-Slot PM-Motors", 0-7803-8987-5/05/$20.00 ©2005 IEEE, pp. 144-148.

[16] Manoj R. Shah and Ayman M. EL-Refaie, "End Effects in Multi-Phase Fractional-Slot Concentrated-Winding Surface Permanent Magnet Synchronous Machines", 978-1-4244-2893-9/09/$25.00 2009 IEEE, pp. 3798-3805.

[17] Nicola Bianchi, Silverio Bolognani, Michele Dai Pr, and Giorgio Grezzani, "Design considerations for fractional-slot winding configurations of synchronous machines," IEEE Trans. Ind. Appl., vol. 42, no. 4, pp. 997-1006, Jul./Aug. 2006.

[18] Florence Meier, "Permanent-Magnet Synchronous Machines with Non-Overlapping Concentrated Windings for Low-Speed Direct-Drive Applications", Doctoral thesis, Royal Institute of Technology, Stockholm 2008.

[19] Stephan Meier, "Theoretical design of surface-mounted permanent magnet motors with field weakening capability", Master's Thesis, Royal Institute of Technology, Stockholm 2002.

[20] P. Salminen, "Fractional slot permanent magnet synchronous motors for low speed applications. Doctoral thesis, Lappeenranta University of Technology, Finland, 2004.

[21] Derong Luo, Benquan Cheng, Shoudao Huang and Jian Gao, "Method for Optimize the Air Gap Flux Density of Permanent Magnet Synchronous Motor", IEEE Explore.

[22] Nicola Binachi, "Electrical Machine Analysis using Finite Elements", CRC Press and Tailor & Francis Group, pp.34-35, 167-184.

[23] Jacek F. Gieras and Mitchell Wing, "Permanent Magnet Motor Technology - Design and Applications", Second Edition, Marcel Dekker, Inc., 2002, pp. 1-42,169-226.

[24] PC-BDC 6.5, User's Manual, SPEED Consortium, Department of Electrical Engineering, University of Glasgow, pp. 1-6, September 2004.

[25] Vishal D Devdhar and R H Patel, "Surface Mounted Permanent Magnet Synchronous Motor with Fractional Slot Concentrated Winding: A Review", International Conference in Current Trends in Technology, NUiCONE 2011, Dec 9-11, Ahmedabad, India.

List of Publication

1. Vishal D Devdhar and R H Patel, "Surface Mounted Permanent Magnet Synchronous Motor with Fractional Slot Concentrated Winding: A Review", International Conference in Current Trends in Technology, NUiCONE 2011, Dec 9-11, Ahmedabad, India.